Mon. Not. R. Astron. Soc. **262,** 650–680 (1993)

Line-strength gradients in elliptical galaxies

Roger L. Davies,[1]★ Elaine M. Sadler[2]★ and Reynier F. Peletier[3]

[1] *Department of Physics, Astrophysics Group, Keble Road, Oxford OX1 3RH*
[2] *Anglo–Australian Observatory, PO Box 296, Epping, NSW 2121, Australia*
[3] *European Southern Observatory, K. Schwarzschildstr. 2, 8046 Garching bei München, Germany*

Accepted 1992 November 17. Received 1992 November 12; in original form 1992 July 11

ABSTRACT

We have measured line-strength gradients in Mg_2, $\langle Fe \rangle$ and Hβ for 13 galaxies, using two instruments on the KPNO 4-m telescope. The metal-line strengths are consistent with an average abundance gradient of $\Delta[Fe/H]/\Delta \log r = -0.2 \pm 0.1$, or a reduction in mean metallicity of the stellar population of 40 per cent over a factor of 10 in radius. Although line-strength gradients cannot be simply transformed to metallicity gradients, these values are the same as those inferred from colour gradients. These shallow gradients present a significant challenge to current theories of galaxy formation. The dissipative models of Larson & Carlberg produce gradients that are steeper than those measured in giant ellipticals. On the other hand, models of the formation of ellipticals that rely only on stellar interactions, such as dissipationless hierarchical merging, have no mechanism for the generation of metallicity gradients. White has shown that an *existing* gradient would be diluted by about a factor of 2 over three merger events. Together, these considerations support the hypothesis that giant ellipticals form by stellar mergers, and that the line-strength gradients originate in their lower mass progenitors which formed predominantly by dissipational collapse.

We find no correlations between the size of the gradient and any other global parameter of the galaxies, such as luminosity or flattening. Our sample, however, spans only about a factor of 10 in luminosity. We find that the contours of constant line strength have the same shape as the isophotes. The correlations between local colours and local line strengths indicate that dust does not play a significant role in the generation of colour gradients in elliptical galaxies.

We confirm the findings of previous workers that the slope of the $\langle Fe \rangle$ versus Mg_2 relation within ellipticals is steeper than the equivalent relation for the nuclei of ellipticals. This can be interpreted as evidence for an enrichment of Mg over Fe compared to the solar values used in the models. Age differences or a younger population cannot be invoked to account for the difference. Mg could be enhanced with respect to Fe over the solar value in the giant ellipticals either by enhanced early star formation or by skewing of the initial mass function to produce more massive stars. Alternatively, a deficiency of $\langle Fe \rangle$ could be produced if the binary fraction in elliptical galaxies were lower than the local value.

We find that Hβ absorption is constant or increases with increasing radius in almost all of the galaxies we observe. We suggest that this is due to the dilution of the Hβ absorption feature by emission in the centres of these galaxies, an effect which decreases with increasing radius. Our results are consistent with no gradient in the age of the stellar population. We find that the galaxies with the bluest $1550 - V$ colours have the strongest Hβ emission. We speculate that the inverse relationship between Mg_2 and $1550 - V$ might be due to the presence of an otherwise undetected blue ionizing nucleus in galaxies with high values of Mg_2, and that both the activity and the

★ Visiting observer at Kitt Peak National Observatory, NOAO, which is operated by the Association of Universities for Research in Astronomy, Inc., under contract to the National Science Foundation.

high metallicity might result from the star formation associated with the formation of a core.

We investigate the relationship between metallicity and escape velocity proposed by Franx & Illingworth. Their suggestion that metallicity is a function of the *local* escape velocity is confirmed by using a more direct indicator of metallicity and a separate calculation of V_{esc} for each galaxy. While this result supports the view that abundance gradients and the colour–magnitude relation for ellipticals arise from a common physical cause, the decoupling of Mg_2 and $\langle Fe \rangle$ gradients indicates that other effects, depending on the details of the star formation history, are at work.

NGC 4472 and 7626 have anomalous core kinematics and enhanced Mg_2 within their cores. This suggests that the formation of the cores was accompanied by significant star formation activity that generated a high-metallicity population. This high metallicity does not support models in which the anomalous core is the remnant of a captured low-mass galaxy, as even the most metal-rich low-mass galaxies have lower central line strengths than those found in the centres of NGC 4472 and 7626.

Key words: galaxies: abundances – galaxies: elliptical and lenticular, cD – galaxies: formation – galaxies: stellar content.

1 INTRODUCTION

Line-strength gradients in elliptical galaxies have long been proposed as a diagnostic of the processes at work during galaxy formation. Larson (1976) and Carlberg (1985) have shown that elliptical galaxies which form by the dissipative collapse of a gas cloud should have radial metallicity gradients. The steepness of the gradient depends on the physical conditions within the protogalaxy at the time of collapse, so measurements of abundance gradients within galaxies may give clues to the importance of dissipative processes in galaxy formation. Larson's models produce galaxies with very steep metallicity gradients, a factor of 10 reduction for a factor of 10 increase in radius. These are ruled out by previous observations (e.g. Faber 1977), and also by kinematic considerations (e.g. Davies et al. 1983). Carlberg's models include a pressure term associated with the energy input from supernovae during the collapse. This decreases the size of abundance gradients in the final galaxies to a factor of 3 over each decade in radius. On the other hand, models of the formation of ellipticals that rely on stellar interactions, such as dissipationless hierarchical merging, have no mechanism for the generation of metallicity gradients. Mergers of stellar galaxies do alter pre-existing gradients: White (1980) has shown that an existing gradient would be diluted by about a factor of 2 over three merger events.

To understand the evolution of the stellar component of galaxies, we need to explore whether the line-strength gradients seen in present-day galaxies are entirely a product of the old stellar population (and hence a reflection of physical conditions at the time of collapse), or have been affected by more recent star formation. Further, we need to investigate whether the colour–luminosity relation for ellipticals (Sandage & Visvanathan 1978) and the line-strength gradients observed in ellipticals have a common physical origin, as has been suggested by Cohen (1979) and more specifically by Franx & Illingworth (1990).

In the well-studied case of M32, there seems to be little doubt that an intermediate-age population is present. O'Connell (1980) showed that a substantial fraction (15 per cent) of the V light comes from a blue stellar population which he identified as consisting of 5×10^9 yr old main-sequence late-F stars. Burstein et al. (1984, hereafter BFGK) estimated that such stars contribute 25 per cent of the light in V, and analyses by BFGK, Rose (1985) and Bica, Alloin & Schmidt (1990) have strengthened the evidence for a young stellar population in M32. BFGK concluded that the only way to reach a high enough Hβ strength in M32 without producing too blue a $2200-V$ colour was to invoke an intermediate-age population. More recently, Elston & Silva (1992) and Freedman (1992) have detected stars in M32 that have higher bolometric luminosities and redder $J-K$ colours than those in the Galactic Bulge, and have suggested that these stars *are* part of the intermediate-age population.

Few measurements of line-strength gradients in galaxies have been published. In an early study, Faber (1977) measured radial gradients in the Mg_2 index for NGC 4472, two S0 galaxies and the bulge of M31. She concluded that all four objects had similar line-strength gradients when scaled to the light of the galaxy, and reported a tendency for the contours of constant line strength to be flatter than the isophotes, in agreement with Larson's (1976) dissipative models. Efstathiou & Gorgas (1985) measured several indices in the Burstein–Faber system for the elliptical galaxy NGC 5813. They plotted Fe and Hβ indices against Mg_2, and compared the observed radial trends with the relationship for the centres of ellipticals from BFGK and with the measurements of globular clusters given there. They concluded that the metallicity at a radius of $1.25r_e$ in NGC 5813 was as low as $[Fe/H] \approx -0.7$.

More recently, papers by Couture & Hardy (1988), Gorgas, Efstathiou & Arágon Salamanca (1990, hereafter GES), Boroson & Thompson (1991, hereafter BT), Faber, Worthey & Gonzalez (1992, hereafter FWG), Delisle & Hardy (1992) and Davidge (1992) have reported new measurements of line-strength gradients. GES and FWG have noted that the Mg_2, $\langle Fe \rangle$ relation within ellipticals is *different* from that for the nuclei of ellipticals in the sense that

⟨Fe⟩ falls more steeply with radius than would be predicted by the Mg_2, ⟨Fe⟩ relation for nuclei. In general, these authors find no strong correlations between line-strength gradients and galaxy parameters such as total luminosity and stellar rotation (note that often only a limited range in these parameters was explored: Davidge, for example, finds shallower gradients in fast rotators and galaxies with low velocity dispersion). The diversity of gradients which is observed appears to reflect a corresponding diversity in star formation history.

In this paper, we address these issues using high signal-to-noise ratio data taken for kinematic studies, supplemented by spectra taken at higher spatial and spectral resolution. In Section 2 we describe the data reduction, and how the indices were measured, corrected for the effects of resolution and velocity dispersion and transformed to the standard Burstein–Faber system. The line-strength results are presented in Section 3, and in Section 4 the relationships between line strengths and colours are discussed. Section 5 explores the connection of line strength to kinematic parameters, and the conclusions are presented in Section 6.

2 THE DATA

We have measured absorption-line strengths in the spectra of 13 bright elliptical galaxies, chosen because good-quality spectra at four or more position angles were available from the work of Davies & Birkinshaw (1988, hereafter DB). We have used the indices (Mg_2, ⟨Fe⟩ and Hβ) defined by Burstein, Faber and collaborators (BFGK; Faber et al. 1985), who have measured them in Galactic stars, globular clusters and the nuclei of elliptical galaxies. The spectra, taken with the Cryogenic Camera at the KPNO 4-m telescope, allow weak absorption-line features to be measured out to large distances (typically 40–50 arcsec, $\sim 1 r_e$) from the centre of each galaxy.

The Cryogenic Camera spectra have poor spatial resolution, so we observed the inner regions of 12 of the galaxies with a Texas Instruments (TI) CCD on the RC spectrograph at the KPNO 4-m telescope. This allows us to study gradients within the central 1–10 arcsec of each galaxy, and to calibrate all our line-strength measurements on a standard scale. All data reduction was done with the IRAF software package (Valdes 1986).

2.1 Observations with the Cryogenic Camera (Cryocam)

The configuration of the Cryocam used is described by DB; the wavelength range was 3800–6400 Å, with a spectral resolution of 12 Å and a spatial scale of 0.86 arcsec pixel^{-1}. Long-slit spectra were taken at four or more position angles (the photometric major and minor axes plus two or more intermediate axes) in each galaxy. Details of exposure times and slit positions are given in table 2A of DB. The reduction process is described below.

2.1.1 *Flat-fielding*

The first step in reduction was to subtract a bias value calculated from the unilluminated portion of each frame, thus subtracting the dark current as well.

Exposures of a quartz lamp within the spectrograph were taken before and after each galaxy observation. The quartz spectra are assumed to be smooth in wavelength, and can thus be used to map out the small-scale, pixel-to-pixel variations in detector sensitivity. For the 1984 February data, instrumental stability was excellent and an average quartz frame for each night was produced from the (10–12) quartz spectra observed. The 1983 November data showed measurable instrumental shifts through each night, and so a series of five quartz frames, each the mean of two or more exposures, was constructed.

The averaged quartz spectra were flattened and normalized by fitting a cubic spline to the continuum in the wavelength direction and dividing by this fit. The rms amplitude in the resulting flattened ('response') frames represents pixel-to-pixel variations in sensitivity, and was typically 5–6 per cent. The quartz lamp did not illuminate the detector in exactly the same way as did the telescope, so the next step was to correct for possible vignetting in the slit direction, using spectra of the twilight sky taken at the end of each night. Each sky frame was first divided by the appropriate quartz response image. The vignetting along the slit was then determined by interactively fitting a cubic spline in each of five wavelength bins, chosen to exclude strong night sky lines. An output ('illumination') frame was produced by interpolating between the fitted points. The amplitude in this frame represents the relative illumination received by each point on the slit, and the rms variation over the whole detector was typically 2–5 per cent.

The final step in flat-fielding was to multiply each response (quartz) frame by the illumination (sky) frame from the same night and divide each galaxy frame by the result. Based on examination of several flat-fielded quartz frames, the final flat-fielded frames were uniform to better than 1 per cent.

2.1.2 *Wavelength calibration*

The next step was to correct the geometric distortion due to the camera optics and transform the spectra to a logarithmic wavelength scale. Spectra of a He–Ne–Ar comparison lamp, observed before and after each galaxy observation, were checked for instrumental shifts and then added. A 'distortion map' of the whole detector was then prepared from each set of comparison spectra by fitting polynomials in both row and column directions to the positions of 20–25 spectral lines. Later reduction programs required that the galaxy spectra be aligned precisely along the CCD columns, so this alignment was determined using the spectra of standard stars and any necessary corrections were incorporated into the distortion map.

The distortion maps were used to transform each galaxy frame to a $\ln\lambda$ scale covering the wavelength region 3860–6340 Å. The transformed spectra had 1024 pixels in the dispersion direction with $\delta(\ln\lambda) = 4.978 \times 10^{-4}$, and $\delta V = 149$ km s^{-1} (ln pixel)$^{-1}$. The spatial alignment of the transformed spectra was accurate to 0.02 pixel, and the rms residual in the spectral fit was typically 0.1–0.2 Å.

2.1.3 *Sky subtraction*

The sky level was determined from the outer parts of each galaxy frame. Spectra covering about 10 arcsec at either side

of the frame, and as far as possible from the centre of the galaxy, were summed to produce a mean 'sky' spectrum, and a linear interpolation between the mean counts at each edge produced a final sky frame which was subtracted from the galaxy frame.

There are two main sources of error in the sky-subtraction process. One is the uncertainty in setting the sky level at any point in the frame, because we have used an interpolation from the outer parts of each frame. The second uncertainty arises because most of the galaxies observed are large enough to fill a large part of the data frame, so that a 'sky' spectrum measured at the edges of the frame contains a contribution from the light of the outer parts of the galaxy as well as from the sky.

As an example, consider the worst case: the major axis spectrum of NGC 4472, the largest galaxy we observed, with an effective radius (r_e) of 99 arcsec. We measured the 'sky' spectrum in two bins, each centred 112 arcsec (or $1.14r_e$) from the nucleus of the galaxy. From CCD photometry by Peletier et al. (1990, hereafter PDIDC), the B surface brightness of the galaxy at the position of the 'sky' bins is 22.9 mag arcsec^{-2}, corresponding to a V surface brightness of 21.9 mag arcsec^{-2} with $B-V=1.0$. Since the sky brightness at Kitt Peak is typically $V=21.9$ mag arcsec^{-2} on a dark night, up to 50 per cent of the subtracted 'sky' spectrum for NGC 4472 actually consists of light from the outer regions of the galaxy. More typically, for NGC 4278 with $r_e=30$ arcsec, the galaxy contributes about 15 per cent of the light in the 'sky' spectrum.

We tested the effects of contamination of the sky spectrum in NGC 4472 by constructing an independent (and much less contaminated) 'sky' spectrum from the outer regions of frames containing stars and the smallest galaxies. We looked at the brightness profile of NGC 4472 integrated along the spectrum from 4800 to 5500 Å, and scaled the sky spectrum so that, when it was subtracted from the galaxy spectrum, the residual profile fitted the photometric surface brightness profile. We then measured the line-strength indices for this sky-subtracted galaxy spectrum, and we also over- and under-subtracted the sky spectrum. In practice, contamination of the 'sky' spectrum by galaxy light had little or no effect on the measured line-strength indices. For NGC 4472, line strengths measured up to 60 arcsec out (the largest distance for which reliable values could be measured) had the same value when the sky subtraction was done using the edges of the same frame as when a correctly scaled, uncontaminated sky spectrum was used. The errors introduced are small because the line-strength gradients in general are very small. The signal-to-noise ratio is lower when sky spectra are taken from the galaxy frame, because we also remove some galaxy light in the outer parts. For NGC 4472, about 25 per cent of the galaxy light 60 arcsec out is lost in this way.

The flux in the final, sky-subtracted spectrum at a distance r from the centre of the galaxy is given by

$$F_{gal}(\lambda, r) = F_{obs}(\lambda, r) - [F_{sky}(\lambda, r_{sky}) + F_{gal}(\lambda, r_{sky})],$$

where r_{sky} is the distance at which the sky spectrum is measured, and only errors in F_{sky} systematically affect the measured line strengths. We found empirically that an error of 5 per cent in the adopted sky value F_{sky} altered the measured Mg and Fe line strengths in NGC 4472 by 5–7 per cent in the outer parts of the galaxy where the surface brightness was close to that of the sky, and by much less nearer the centre of the galaxy. In practice, the sky level in an individual frame can be determined to better than 5 per cent, and since each galaxy was observed at four or more position angles there are at least four independent sky measurements available. Uncertainties in the subtraction of the sky background are therefore unlikely to be a significant source of error in our data. This is confirmed by the good agreement between line indices measured from independent observations of the same galaxy at the same position angles and of round galaxies at several position angles.

2.1.4 *Cryocam focus gradient*

The Cryogenic Camera suffers from a focus variation which means that lines are broader at the red and blue ends of each spectrum than in the middle. If left uncorrected, this will affect the measured values of indices like Mg_2, where the sidebands cover a relatively large wavelength range, since light from the nucleus spills over into the surrounding regions in a wavelength-dependent way. The effect is noticeable only in the central regions of a galaxy, where the light varies most steeply. We did not attempt to correct for the focus variation at the data reduction stage, but incorporated a broadening correction into the line-strength measurements as described in Section 2.5.2.

2.1.5 *Final Cryocam spectra*

Reduced spectra at various positions along the major axis of NGC 3379, shown in Fig. 1, illustrate the quality of the Cryocam data. Since the spectra are not flux-calibrated, the final continuum shape is determined partly by the instrumental response of the detector. This is not a problem when measuring line-strength gradients within galaxies, since all spectra are affected in the same way, but means that a conversion factor may be needed to compare the results with those of other observers using different instruments.

2.2 Observations with the TI CCD

Observations were made on 1987 April 21–24 and November 17–18 with an 800 × 800 Texas Instruments CCD on the RC spectrograph at the Kitt Peak 4-m telescope. The wavelength range was 4750–6150 Å, with a spectral resolution of 6 Å FWHM and a spatial scale of 0.467 arcsec pixel^{-1}. The slit width was 230 μm, or 1.5 arcsec. The CCD chip was preflashed to a level of about 40 ADU above bias before each galaxy exposure. Spectra of a He–Ne–Ar comparison lamp, and of a quartz flat-field lamp, were taken either before or after each galaxy spectrum. Each afternoon, a series of flat-field spectra was taken using a uniformly illuminated 'white spot' in the telescope dome, and flat-field exposures of the twilight sky were made at the beginning or end of each night's observations.

Table 1 gives the log of observations. Useful data were obtained on six nights, and the seeing was 2–3 arcsec FWHM on April 21 and 22, 1.7 arcsec on April 23, 0.8–1.3 arcsec on April 24, 1–1.5 arcsec on November 17 and 1 arcsec on November 18. Where possible, spectra were taken along both the major and minor axes of each galaxy. Several

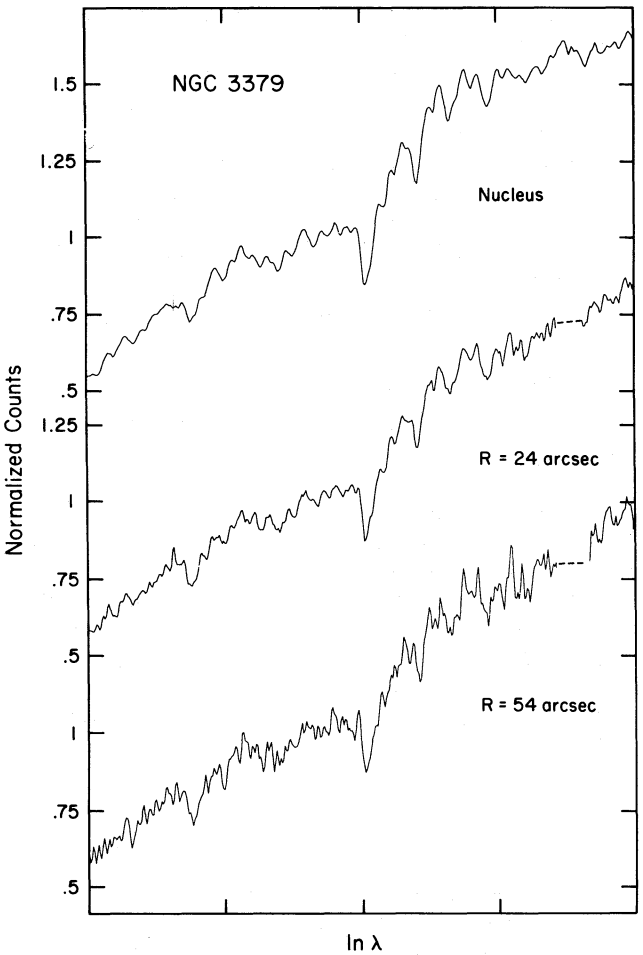

Figure 1. Cryocam spectra of the centre of NGC 3379, and at radii of 24 and 54 arcsec. The abscissa is in intervals of ln λ, so a wavelength scale is inappropriate. For reference, the Mg b absorption feature is at the centre and Hβ is the strongest absorption at shorter wavelengths. The dashed line represents interpolation across the 5577-Å sky emission line.

K-giant template stars (radial velocity standards) were observed on each night.

2.2.1 *Reduction of the TI data*

The TI spectra were reduced in the same way as were the Cryocam data. The CCD chip had been UV-flooded to enhance its blue sensitivity, and as a result the sensitivity was higher at the edges of the chip than in the centre, with large sensitivity variations at the corners. A series of dome flat-fields showed that this did not affect the region of the chip illuminated by the sky.

The bias level in each frame was calculated from an area illuminated by the pre-flash but not by the sky, so the bias and pre-flash spectrum were subtracted at the same time. Since the pre-flash illumination was not completely uniform across the chip, a 'residual pre-flash' frame representing the mean of 10 or so bias-subtracted bias frames was used to subtract the pre-flash light completely. The level of 'residual pre-flash' was small, typically 1–2 ADU.

Table 1. Log of observations with the TI CCD.

Date	Galaxy	Exp.	PA_{obs}	PA_{maj}	ϵ
17 Nov 1987	NGC 315	3000s	133°	43°	.27
17 Nov 1987	NGC 741	3600s	100°	87°	.16
17 Nov 1987	NGC 1600	3600s	82°	172°	.33
18 Nov 1987		3600s	172°		
22 Apr 1987	NGC 3379	1000s	70°	71°	.08
		1000s	160°		
24 Apr 1987		1800s	70°		
22 Apr 1987	NGC 3665	1500s	25°	26°	.23
		1500s	115°		
24 Apr 1987		1800s	25°		
22 Apr 1987	NGC 4261	1000s	160°	159°	.20
		1000s	70°		
24 Apr 1987		1800s	160°		
22 Apr 1987	NGC 4278	1000s	110°	18°	.14
		1000s	20°		
24 Apr 1987		1800s	110°		
23 Apr 1987	NGC 4374	1000s	130°	126°	.16
		1800s	40°		
24 Apr 1987		1800s	130°		
21 Apr 1987	NGC 4472	1200s	70°	162°	.17
23 Apr 1987		1000s	70°		
		1000s	160°		
24 Apr 1987		1800s	160°		
23 Apr 1987	NGC 4486	1000s	160°	157°	.04
		1000s	70°		
24 Apr 1987		1800s	160°		
23 Apr 1987	NGC 4636	1000s	60°	155°	.08
		1000s	150°		
24 Apr 1987		1800s	150°		
17 Nov 1987	NGC 7626	3000s	12°	8°	.11
		3600s	102°		

Flat-fielding and correction for the slit illumination profile were done in the same way as for the Cryocam data. The quartz flat-field frames showed an rms variation of about 4 per cent over the whole chip, which was reduced to less than 1 per cent after flat-fielding.

The wavelength calibration was accurate to 0.1–0.2 Å, and the alignment of the final spectra (as measured by the positions of arc lines after correction by the distortion map) was accurate to ± 0.2 pixel (or better than 0.1 arcsec). The reduced spectra were converted to a ln λ scale, with $\delta(\ln \lambda) = 2.524 \times 10^{-4}$, $\delta V = 75.7$ km s^{-1} (ln pixel^{-1}), and sky subtraction was carried out in the same way as for the Cryocam data.

2.3 Measurement of line-strength indices

There are three stages in the measurement process. First, we need a well-defined way to measure the strengths of various absorption features at different places in a galaxy, and for this we have used a system of line-strength indices defined by Faber et al. (1985). Secondly, if the galaxy has a radial gradient in stellar velocity dispersion (as most elliptical galaxies do), each index must be corrected to the value it would have if measured at some constant velocity dispersion. Since the effect of the internal velocity dispersion is to weaken most of the lines, it is convenient to correct all indices to the values they would have if measured in a single star (i.e. with zero velocity dispersion). After this step, it is valid to compare the strengths of lines measured at different

radii in the same galaxy, or in different galaxies observed with the same instrument. Thirdly, since the measured indices depend on spectral resolution as well as on the spectral response of the detector used, we need to reduce all our measurements to a standard zero-point, so that we can compare line strengths in the galaxies we have observed with those of galaxies, globular clusters and Galactic stars measured by other observers.

2.3.1 *Definition of the indices*

In the system defined by Faber et al. (1985), some indices (Fe, Hβ, Na D) are the equivalent width of the appropriate line (using a continuum level from precisely specified sidebands), while others are defined by the ratio of line depth to continuum level (in magnitudes). We chose to adopt the system exactly as defined by Faber et al. so that we could tie our results to the extensive library of Galactic stars, globular clusters and galaxy nuclei already observed.

The bands defined for Hβ, Mg_2, Fe1 (5270 Å) and Fe2 (5335 Å) are shown in Fig. 2. Several other indices fell within the wavelength range of the Cryocam spectra but were not included in the analysis: the Na D lines suffered severe contamination from a strong night sky feature which crept in and out of the continuum sideband as the focus varied, and the CN and G-band features at the blue end of the spectrum are weak (because of poor instrumental sensitivity in the blue) and suffer severely from the differential focus problem. For the TI spectra, we were able to measure Hβ, Mg_1, Mg_2, Fe1 and Fe2 in the central regions of each galaxy, as well as Na D and TiO1 which are not presented in this paper.

2.3.2 *Correction of the Cryocam focus gradient*

To correct for the focus problem, the Cryocam data were smoothed along the slit in such a way that the smoothed spectra in the centre accurately represent the light of the galaxy at a single radius. A Gaussian of FWHM typically 3–4 arcsec was required, so that the spatial resolution in the centre is degraded. The required smoothing was determined individually for each index in each galaxy. The wavelength bins used to calculate each index were shifted to correspond to the galaxy redshift determined by DB.

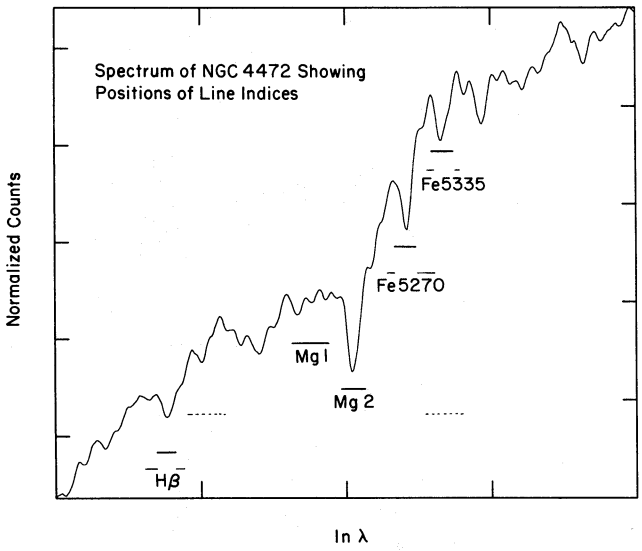

Figure 2. The Lick indices used in this paper. Solid lines indicate the features; dashed lines indicate the continuum bands.

2.3.3 *Line-strength indices from the two data sets*

Fig. 3 shows the radial variation of the Mg_2, Fe 5270-Å and Hβ indices for all 13 galaxies before correction for velocity dispersion. Values in the inner regions of each galaxy were averaged over 3–5 arcsec, and those further out averaged over larger regions of up to 10–12 arcsec. The radius is plotted as r/r_e^*, where $r_e^* = r_e(1-\varepsilon)^{1/2}$ along the minor axis, $r_e^* = r_e(1-\varepsilon)^{-1/2}$ along the major axis and $r_e^* = r_e$ along intermediate axes; r is the radial distance from the centre of the galaxy, ε the ellipticity and r_e the de Vaucouleurs half-light radius (i.e. the radius of a circular aperture which contains half the total light of the galaxy). The profiles have been folded about the centre of each galaxy, and the error bars show the rms scatter in individual values before averaging. The dashed line shows the FWHM of the Gaussian used to smooth the data before measuring the indices, and our data contain no spatial information to the left of this line.

2.3.4 *Line strengths along major and minor axes*

There is no significant variation of line-strength gradient with position angle for any of the galaxies in Fig. 3, and contours of constant line strength appear to have the same shape as the stellar isophotes (though the sample contains no highly flattened galaxies, in which deviations might be more obvious). We have therefore averaged the values from all position angles to give a single set of line-strength measurements for each galaxy. Quantitative attempts to fit the shape of ellipses of constant line strength to the measurements at representative surface brightness confirm that these have the same flattening as the isophotes. Note that in Fig. 3 the radius r is measured along the *intermediate* axis of each galaxy. GES also found no significant difference between the major and minor axis gradients in Mg_2 or other indices for the three galaxies that they observed along both axes.

2.4 Correction for velocity dispersion

The next step was to correct the measured indices for the effects of line broadening due to the internal velocity dispersion of each galaxy. We used broadened stellar templates to derive an empirical correction factor, $C(\sigma)$, such that $C(\sigma) = \text{index}(0)/\text{index}(\sigma)$.

Spectra of several G8–K1 giant stars were used to calculate the velocity dispersion correction. The stars were assumed to have zero intrinsic velocity dispersion, and their spectra were broadened using a series of Gaussian filters with $\sigma = 50$, 100, 150, 200, 250, 300 and 350 km s^{-1} (matching the observed range of σ in the programme galaxies). The correction factor $C(\sigma)$ was then calculated for each index. The scatter in $C(\sigma)$ at large σ was 1–2 per cent for Mg_2 and 5–6 per cent for Fe, and is probably due largely to instrumental effects, since the scatter between different observations of the same star was as large as that between spectra of different stars. However, we checked for a

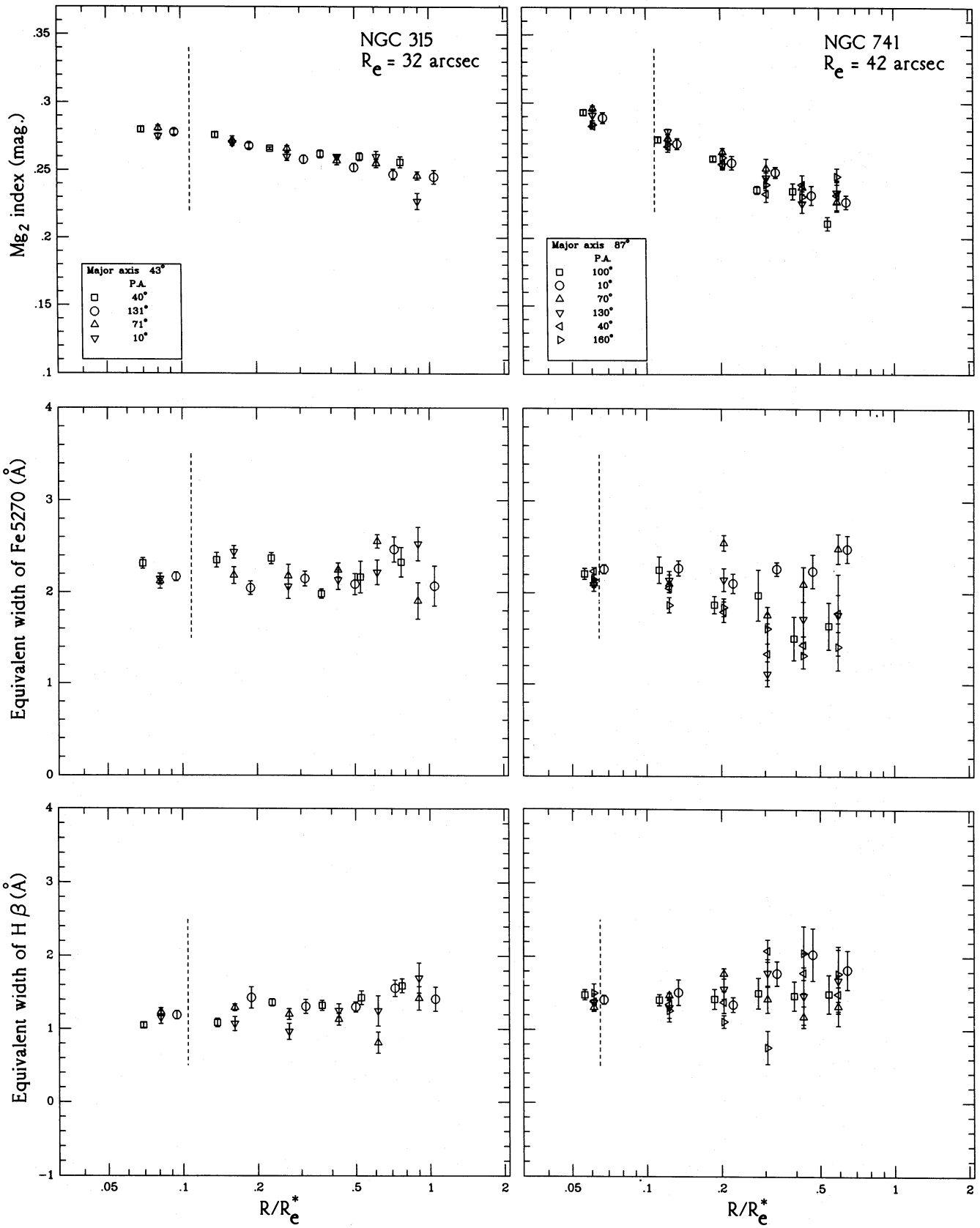

Figure 3. Uncorrected Cryocam data at four position angles per galaxy. See text for a definition of r_e^*. These indices have not been corrected for velocity dispersion broadening.

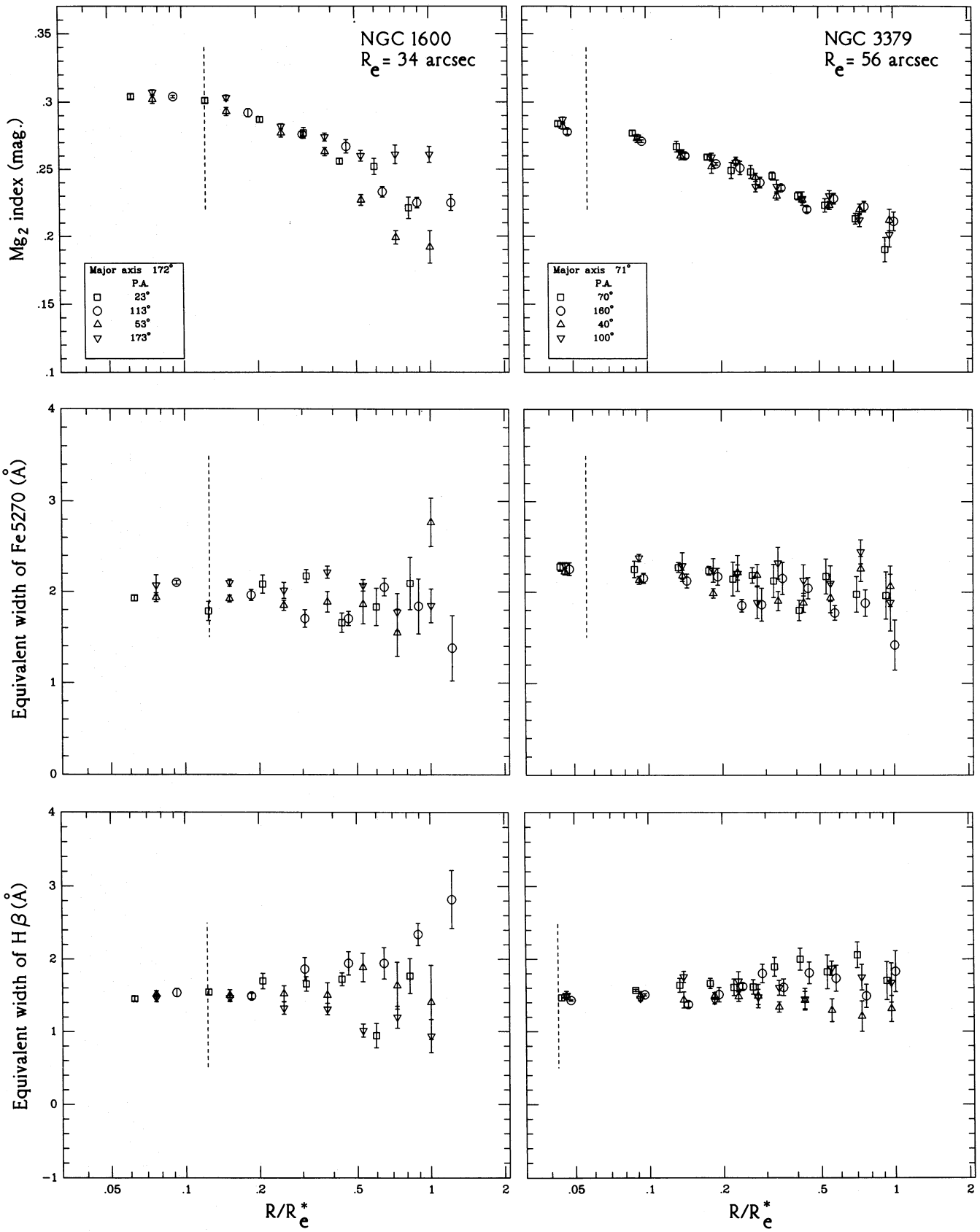

Figure 3 – *continued*

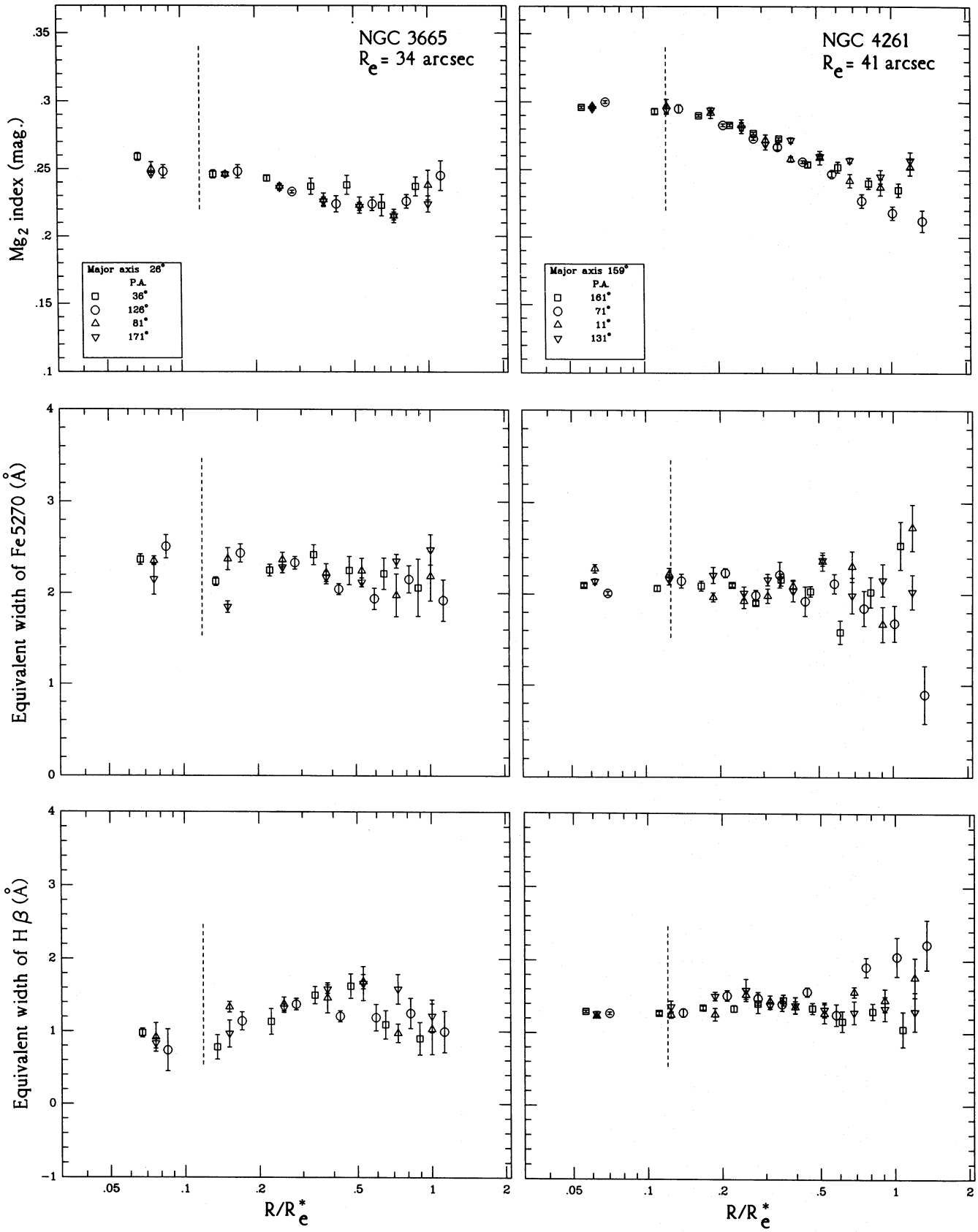

Figure 3 – *continued*

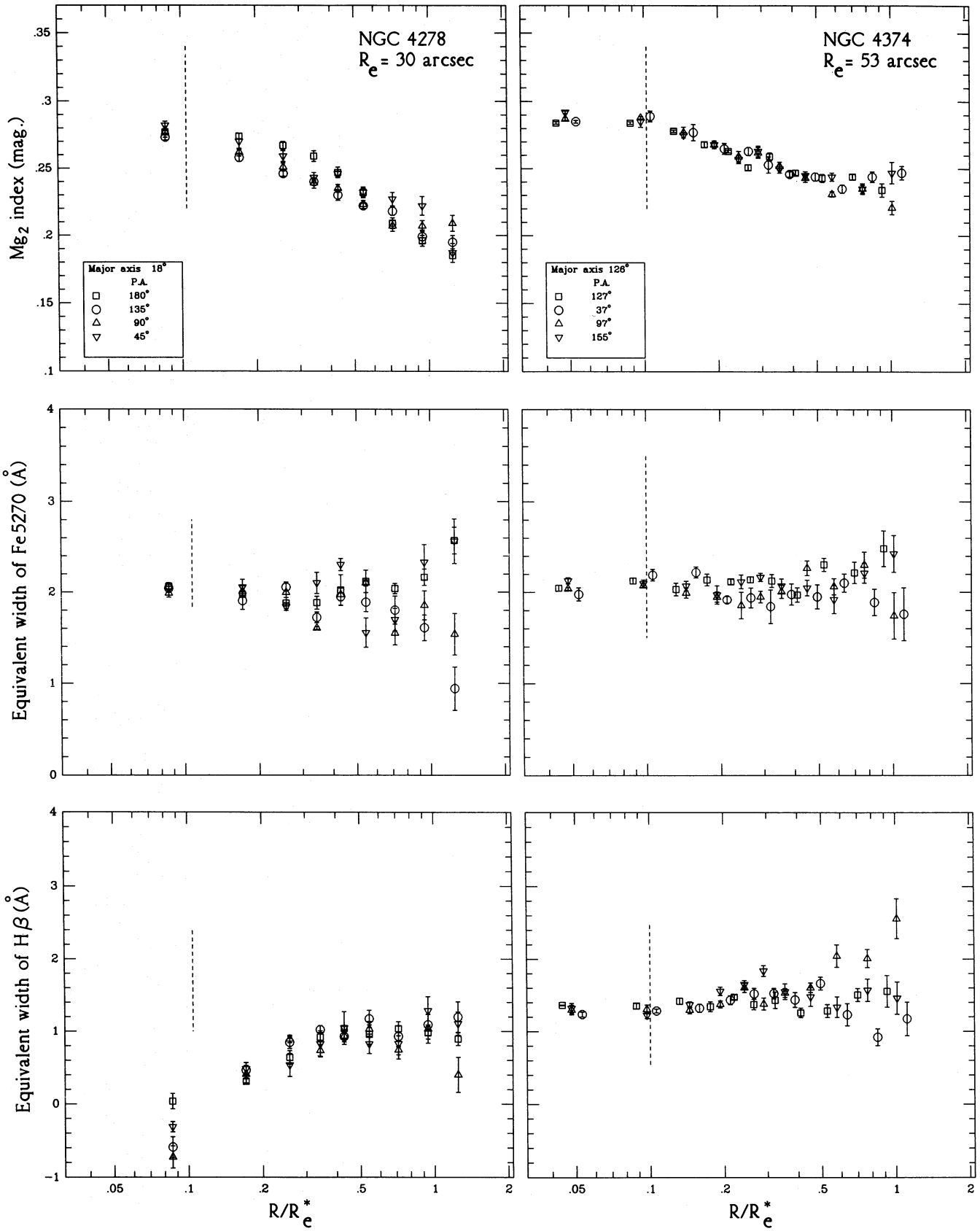

Figure 3 – *continued*

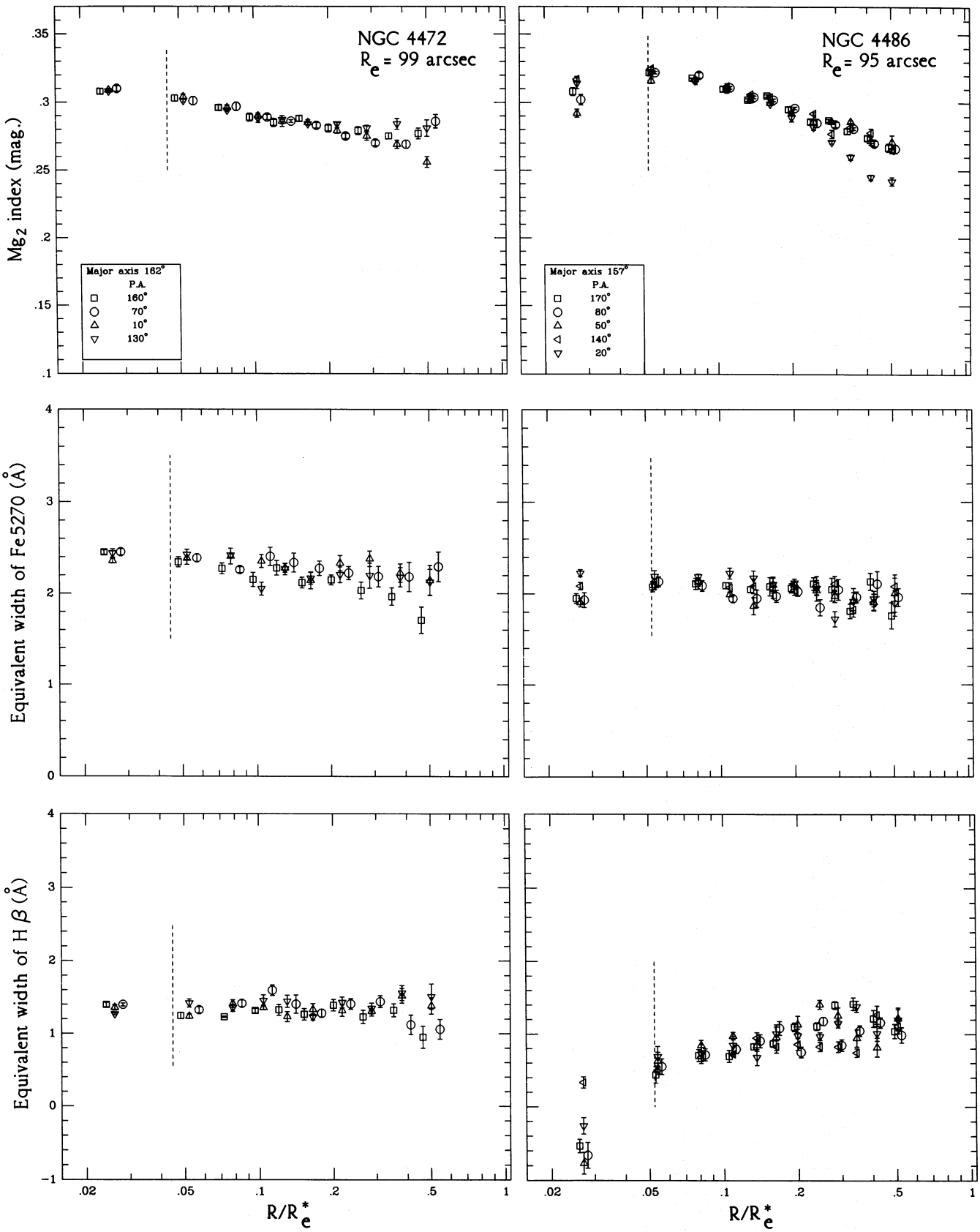

Figure 3 – *continued*

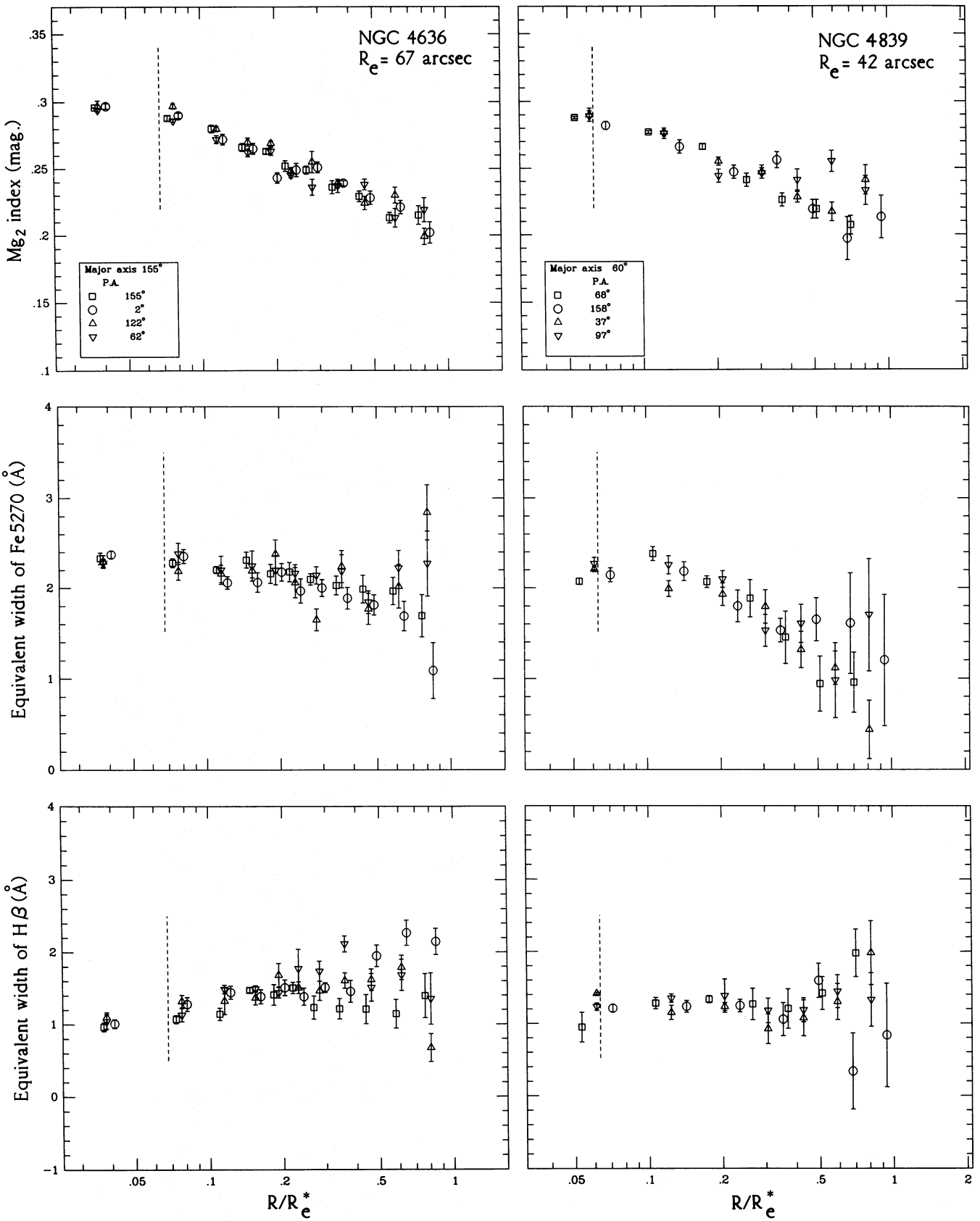

Figure 3 – *continued*

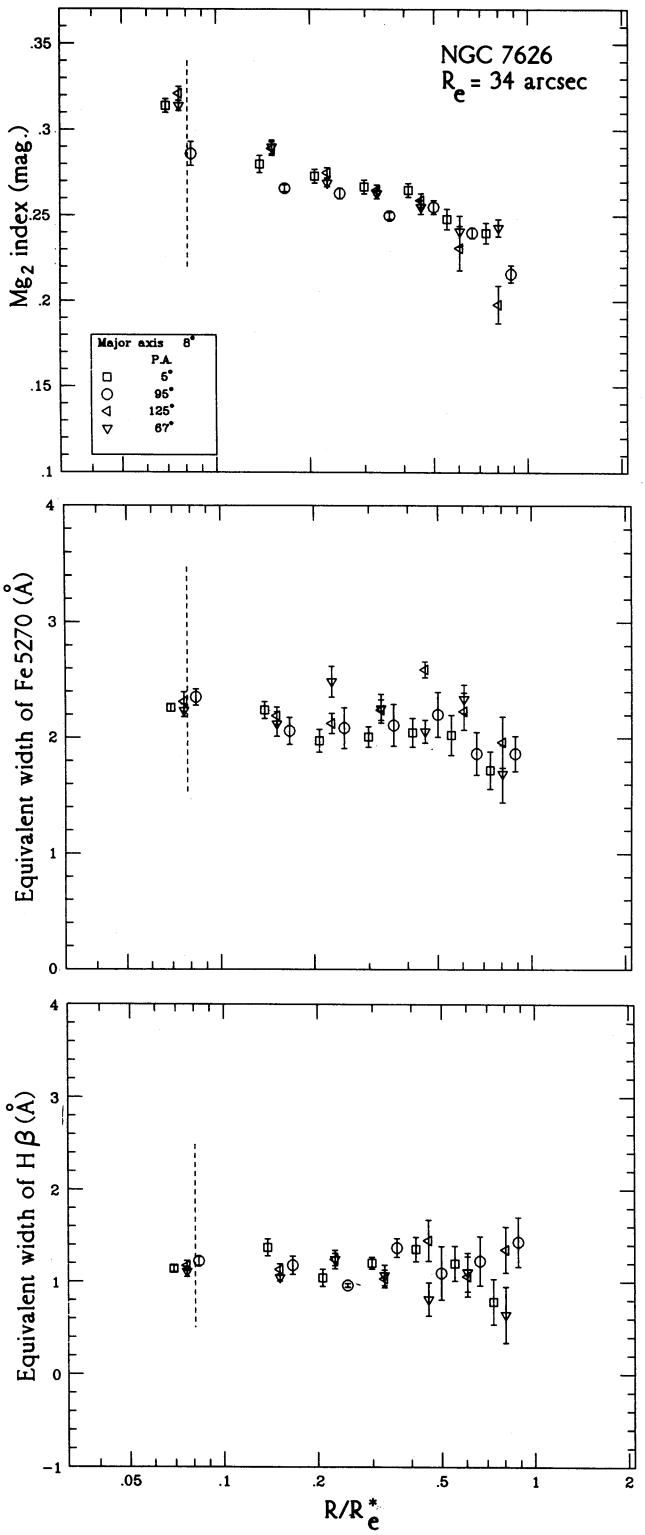

Figure 3 – *continued*

dependence of the correction factor $C(\sigma)$ on metallicity. For Mg_2, there was some evidence that the correction factor was larger for the weakest lined stars, but for stars that spanned the range in Mg_2 seen in the galaxies ($Mg_2 > 0.18$) there was no evidence for a variation with metallicity. The same was true of the Hβ and Fe indices.

The final adopted $C(\sigma)$ was found by taking the mean of the measured correction factors for the eight strong-lined stars which were tested. Separate correction factors were calculated for the Cryocam and TI spectra. A bicubic spline interpolation between the tested values of σ produced a table of $C(\sigma)$ for $0 < \sigma < 350$ km s^{-1}. Fig. 4 shows the adopted correction factors in each index for the Cryocam and TI data. In general, the measured line strengths *decrease* with increasing σ. The change is small for the Mg and Hβ indices, but can be substantial (up to 50–60 per cent) for the weaker Fe lines.

The galaxy indices were corrected for velocity dispersion by assuming that σ within each galaxy varied linearly between the central value σ_0 and the value at r_e, σ_e, as measured by DB. Table 2 lists the values of σ_0 and σ_e adopted for each galaxy.

2.5 Conversion to the Lick scale

Two effects must still be accounted for: the difference in spectral resolution between our data and those of Faber et al., and the different spectral response functions of the Lick IDS (for which the Faber indices are defined), the Cryogenic camera and the UV-flooded TI CCD.

We chose to combine these two corrections, and adopted a 'bootstrap' procedure to convert the Cryocam and TI indices to the Lick scale. Since the TI spectra have good spatial resolution, we first converted the TI indices to the Lick scale by comparing values within a central 1.5×4.0 arcsec^2 aperture. We then compared the TI and Cryocam indices within a larger (1.5×10 arcsec^2) aperture, and converted the Cryocam indices to the Lick scale via the TI data. This is necessary because the spatial resolution of the Cryocam data is too low for a direct comparison with the small-aperture Lick measurements.

2.5.1 *Zero-point correction for the TI data*

We first measured line indices from the TI spectra, using a bin 9 pixel wide and centred at the centre of the galaxy. This corresponds closely to the 1.4×4.0 arcsec^2 aperture used by Faber et al. The TI indices were corrected for velocity dispersion, and were then compared with single-aperture measurements of the same galaxies observed with the Lick IDS by Faber et al. (Gonzalez, private communication). We corrected the Lick values for velocity dispersion using empirical correction formulae derived by C. Morea (also communicated to us by Gonzalez), and we used the same values of central velocity dispersion as were used to correct the TI data (Table 2). The Lick velocity dispersion corrections are qualitatively similar to those shown in Fig. 4.

For the Fe, Na and Hβ indices, we determined a conversion factor [index(Lick)/index(TI)] for each observation. For the Mg indices, which are measured in magnitudes, we took the difference [index(Lick) − index(TI)]. In general, the correction factors for galaxies in our sample were independent of line strength, velocity dispersion and galaxy redshift, though there is a weak dependence on σ for the two Fe indices. The mean correction factors are listed in Table 3. Most of the difference between the TI and Lick scales is due to a difference in spectral response, not spectral resolution, so that the Mg indices, which have widely spaced continuum bands, have the largest correction factor.

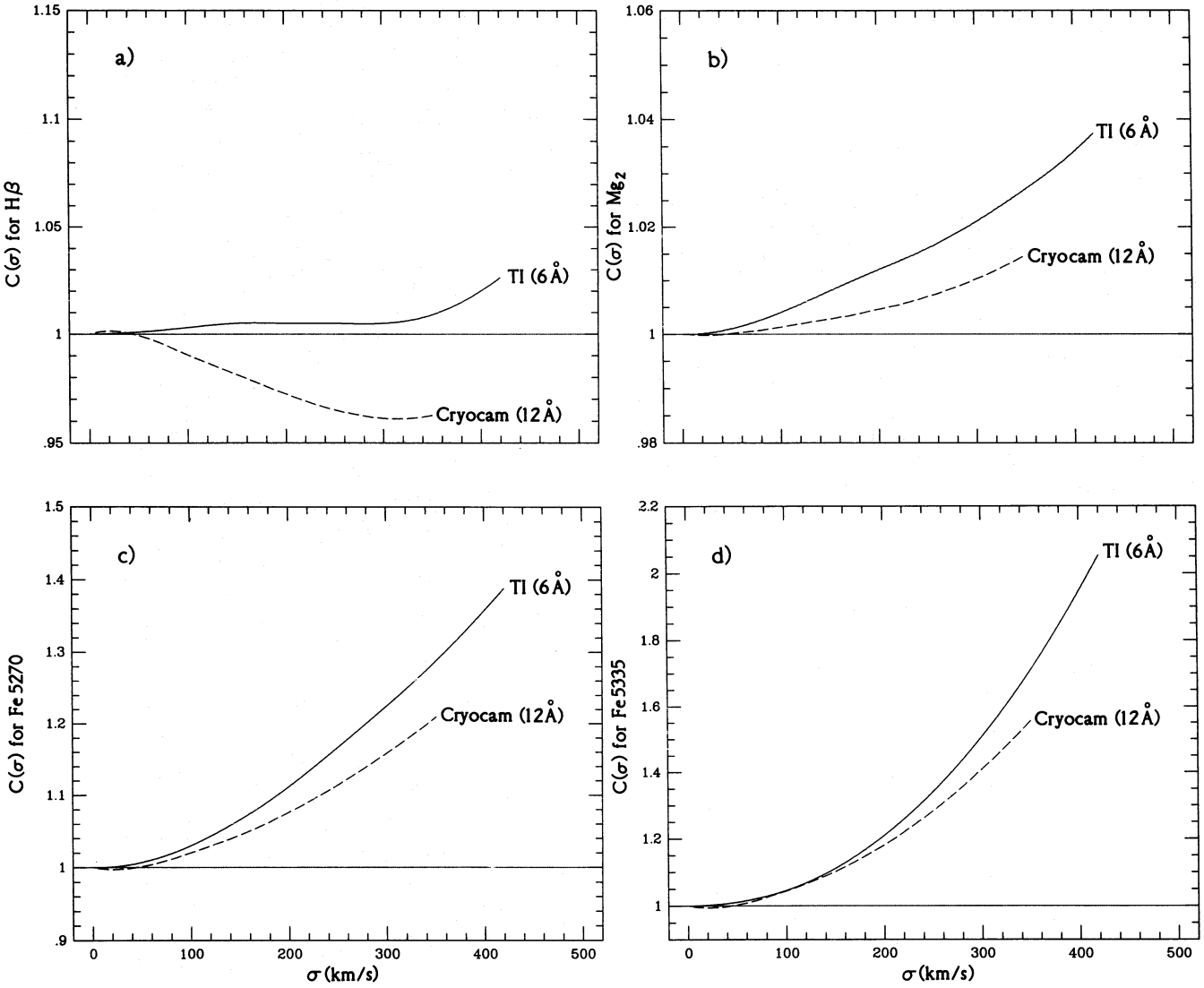

Figure 4. Velocity dispersion correction factors $C(\sigma)$ for each line index for the TI and Cryocam data. See Section 2.4.

2.5.2 *Zero-point correction for the Cryocam data*

We calculated conversion factors between the Cryocam and Lick scales in the way described above, this time comparing the measured indices for Cryocam and corrected TI data within an aperture of approximately 1.5×10 arcsec^2. In contrast to the TI–Lick corrections, most of the change in the Cryocam indices comes from the lower spectral resolution rather than from differences in spectral response. Resolution changes affect the indices in the same way as do changes in the galaxy velocity dispersion, so the iron indices are most strongly affected. The Cryocam–Lick correction factors are also listed in Table 3.

Table 4 lists the final corrected line-strength indices for each galaxy. These correspond to a spectral resolution of 9 Å and zero internal velocity dispersion. The tabulated uncertainties were deduced from the scatter in determinations of the line strengths in each radial bin on both sides of the galaxy centre. For galaxies with redshifts above 4500 km s^{-1}, the Fe2 index is unreliable because of contamination by the strong 5461-Å mercury line from Tucson street lights. For the four galaxies affected, NGC 315, 741, 1600 and 4839, Fe2 is omitted from Table 4. For the most distant galaxy in the sample, NGC 4839, both Fe1 and Fe2 were contaminated, so only the Mg and Hβ indices are listed.

3 LINE-STRENGTH GRADIENTS

3.1 The determination of line-strength gradients

Fig. 5 shows the radial variation of Hβ, $\langle$Fe$\rangle$ and Mg_2 in each galaxy. Since the line-strength indices vary smoothly with radius, the values of Mg_1, Mg_2, $\langle$Fe$\rangle$ and Hβ from Table 4 were fitted by linear regression to $\log(r/r_e)$ to generate the gradients given in Table 5. Points at radii of less than 3 arcsec were excluded from the fits, as they are affected by seeing.

Table 5 lists the slope Δindex/$\Delta\log(r)$, the intercept at r_e and the formal errors in the fit.

3.2 Gradients in Mg

The mean Mg_2 gradient for the 13 galaxies observed here is -0.059 (± 0.022), which agrees well with the values of -0.058 ± 0.027 for the ellipticals in the GES sample and -0.053 ± 0.015 for the six early-type galaxies observed by Couture & Hardy (1988). Davidge (1992) has found a steeper mean gradient of -0.081 ± 0.012 for a sample of 11 ellipticals.

Line-strength gradients have been measured for NGC 4472 by Faber (1977), BT and GES. Their values are plotted in Fig. 6, together with our own data. There is good correspondence between the Mg_2 measurements from the TI CCD, Cryocam, BT (excluding the last point) and Faber (1977). The GES Mg_2 profile, however, has a somewhat different shape, and GES measured a steeper gradient (-0.042 ± 0.007) than our value of -0.028 ± 0.003.

Table 2. Adopted velocity dispersion profiles.

Galaxy	r_e (arcsec)	$\sigma(0)$ (km s^{-1})	$\sigma(r_e)$ (km s^{-1})	M_B
NGC 315	32	314	314	−22.6
NGC 741	42	300	300	−22.8
NGC 1600	34	332	230	−22.9
NGC 3379	56	231	120	−20.6
NGC 3665	34	205	205	−21.6
NGC 4261	41	320	260	−21.7
NGC 4278	30	243	200	−19.2
NGC 4374	53	298	232	−21.5
NGC 4472	99	310	240	−22.4
NGC 4486	95	336	230	−22.1
NGC 4636	67	227	227	−20.6
NGC 4839	42	269	269	−23.2
NGC 7626	34	270	270	−22.1

Sources of data for Table 2. r_e is from the Second Reference Catalogue of Bright Galaxies (de Vaucouleurs et al. 1976). For NGC 3665, we took $r_e = D(0)/6$. Central velocity dispersions are from Davies et al. (1983), except for NGC 4261 (Davies & Birkinshaw 1988), NGC 741 and NGC 3665 (Whitmore et al. 1985). Values at r_e are estimates from the Cryocam data.

Table 3. Correction factors for indices to the Lick scale.

Index	Correction factor	
	TI CCD	Cryocam
Fe1	$\times(0.00110\sigma + 0.694)$	×1.199
Fe2	$\times(0.00104\sigma + 0.771)$	×1.545
Hβ	×1.036	×1.080
Mg1	+0.023 mag.	+0.024 mag.
Mg2	+0.017 mag.	+0.031 mag.

Couture & Hardy observed one galaxy in common with our work, NGC 3379. Their data are considerably noisier than ours, but their measured gradient, -0.064 ± 0.042, agrees well with our value of -0.065 ± 0.003. For the four galaxies Davidge observed in common with our sample, the measurements for two, NGC 741 and 4278, are in good agreement with our data, while for two, NGC 3379 and 4486, Davidge measured substantially steeper gradients. Neither Couture & Hardy nor Davidge have standardized their measurements to a common resolution or corrected for the effects of velocity dispersion. These factors are small for the Mg_2 index, however, and cannot explain the discrepancy with Davidge. We note that Davidge's measurements are discrepant in the largest galaxies we have in common.

3.3 Gradients in Fe

We measured radial ⟨Fe⟩ profiles for nine galaxies. The mean ⟨Fe⟩ gradient of -0.38 ± 0.26 is lower but not significantly different from the mean of -0.58 ± 0.35 quoted by GES for a combined sample of elliptical, cD and S0 galaxies, but it is significantly shallower than the mean of -0.87 ± 0.31 found by Davidge (1992).

Table 4. Final corrected indices.

r_{int} (")	log r/r_e	Mg_1 (mag)	±	Mg_2 (mag)	±	Fe1 (Å)	±	Hβ (Å)	±	Instr.
NGC 315				V_h = 4924 km/s			r_e = 32 arcsec			
0.7	−1.660	0.176	.002	0.315	.003	3.14	.16	0.49	.19	T
3.7	−0.937	0.162	.002	0.320	.002	2.98	.09	1.53	.08	T
5.1	−0.798	0.151	.001	0.306	.001	3.17	.11	1.27	.08	C
8.5	−0.576	0.146	.003	0.297	.002	3.08	.08	1.26	.08	C
9.7	−0.518	0.154	.003	0.299	.005	2.80	.15	1.80	.12	T
13.6	−0.372	0.140	.002	0.292	.002	2.97	.07	1.30	.04	C
17.3	−0.267	0.143	.006	0.298	.009	3.55	.24	1.83	.28	T
19.7	−0.211	0.131	.004	0.289	.003	3.31	.12	1.31	.15	C
28.7	−0.047	0.120	.006	0.278	.005	3.10	.17	1.59	.06	C
NGC 741				V_h = 5457 km/s			r_e = 42 arcsec			
0.5	−1.924	0.157	.003	0.309	.003	3.54	.12	1.11	.12	T
3.3	−1.105	0.149	.003	0.298	.003	3.05	.07	1.26	.09	T
5.2	−0.907	0.148	.002	0.306	.001	2.94	.08	1.44	.04	C
8.3	−0.704	0.151	.005	0.256	.005	3.14	.26	0.75	.12	T
8.5	−0.694	0.136	.001	0.292	.001	2.85	.15	1.49	.09	C
12.8	−0.516	0.123	.001	0.277	.003	2.33	.22	1.62	.18	C
14.9	−0.450	0.147	.005	0.243	.007	1.89	.42	0.95	.21	T
18.0	−0.368	0.126	.002	0.267	.002	2.39	.19	1.73	.14	C
24.8	−0.229	0.121	.005	0.263	.004	2.68	.23	1.66	.07	C
34.1	−0.090	0.110	.009	0.246	.012	2.09	.59	1.88	.29	C
NGC 1600				V_h = 1600 km/s			r_e = 34 arcsec			
0.4	−1.929	0.173	.001	0.337	.005	3.43	.05	1.62	.05	T
1.4	−1.385	0.175	.003	0.340	.002	3.12	.06	1.62	.04	T
3.7	−0.963	0.172	.008	0.332	.007	2.91	.11	1.51	.05	T
5.1	−0.824	0.167	.001	0.331	.002	2.74	.08	1.56	.02	C
7.8	−0.639	0.150	.007	0.303	.007	3.42	.15	1.80	.12	T
8.5	−0.602	0.158	.001	0.314	.002	2.67	.10	1.66	.10	C
12.8	−0.424	0.150	.003	0.304	.003	2.76	.15	1.67	.12	C
13.9	−0.388	0.150	.006	0.295	.008	3.08	.20	1.69	.18	T
17.9	−0.279	0.135	.002	0.277	.007	2.61	.12	1.71	.19	C
24.8	−0.137	0.124	.003	0.267	.012	2.35	.08	1.59	.28	C
34.0	0.000	0.119	.006	0.257	.012	2.66	.33	1.81	.36	C

Table 4 – *continued*

NGC 3379 V_h = 922 km/s r_e = 56 arcsec

r_{int} (")	log r/r_e	Mg_1 (mag)	±	Mg_2 (mag)	±	<Fe> (Å)	±	Fe1 (Å)	±	Fe2 (Å)	±	Hβ (Å)	±	Instr.
0.5	−2.049	0.165	.003	0.317	.005	3.03	.10	2.99	.10	3.08	.11	1.33	.03	T
1.9	−1.469	0.168	.001	0.310	.001	2.97	.09	3.02	.12	2.93	.06	1.52	.01	T
3.3	−1.230	0.168	.001	0.307	.001	2.84	.07	2.79	.02	2.88	.12	1.60	.01	T
5.2	−1.032	0.161	.001	0.301	.002	2.88	.14	2.84	.11	2.92	.17	1.46	.01	T
5.2	−1.032	0.162	.001	0.307	.001	2.83	.08	2.92	.06	2.75	.09	1.58	.02	C
7.5	−0.873	0.158	.001	0.290	.003	2.89	.08	2.85	.11	2.93	.05	1.54	.10	T
7.7	−0.862	0.155	.002	0.295	.001	2.87	.07	2.89	.04	2.85	.09	1.62	.08	C
10.3	−0.735	0.159	.004	0.286	.001	2.71	.13	2.73	.10	2.69	.17	1.60	.01	T
10.3	−0.735	0.151	.001	0.288	.002	2.80	.05	2.81	.07	2.80	.04	1.60	.05	C
12.9	−0.638	0.148	.001	0.285	.001	2.64	.08	2.73	.10	2.55	.07	1.68	.04	C
14.5	−0.587	0.153	.003	0.278	.004	2.49	.07	2.51	.01	2.47	.14	1.38	.08	T
15.5	−0.558	0.141	.001	0.274	.002	2.73	.08	2.62	.10	2.84	.05	1.68	.07	C
18.9	−0.472	0.133	.002	0.269	.003	2.77	.10	2.74	.10	2.81	.11	1.70	.10	C
24.0	−0.368	0.129	.003	0.258	.002	2.59	.10	2.51	.08	2.67	.12	1.76	.13	C
30.8	−0.260	0.127	.003	0.258	.002	2.48	.13	2.53	.10	2.42	.16	1.78	.12	C
40.9	−0.136	0.124	.002	0.249	.002	2.58	.15	2.69	.14	2.47	.16	1.73	.17	C
53.9	−0.017	0.112	.005	0.235	.004	2.05	.21	2.27	.15	1.83	.26	1.74	.10	C

NGC 3665 V_h = 1882 km/s r_e = 34 arcsec

r_{int} (")	log r/r_e	Mg_1 (mag)	±	Mg_2 (mag)	±	<Fe> (Å)	±	Fe1 (Å)	±	Fe2 (Å)	±	Hβ (Å)	±	Instr.
0.5	−1.833	0.143	.002	0.296	.003	2.75	.09	2.66	.08	2.85	.11	1.12	.11	T
2.3	−1.170	0.134	.001	0.281	.002	2.73	.05	2.78	.07	2.67	.03	1.10	.01	T
4.7	−0.859	0.123	.001	0.272	.002	2.53	.17	2.71	.15	2.35	.18	1.00	.09	T
5.1	−0.824	0.133	.001	0.279	.001	2.75	.22	2.85	.15	2.65	.29	1.11	.10	C
7.5	−0.656	0.122	.002	0.272	.006	2.51	.05	2.64	.05	2.38	.05	1.24	.27	T
8.5	−0.602	0.122	.003	0.269	.002	2.88	.04	2.99	.03	2.76	.06	1.37	.05	C
11.6	−0.467	0.121	.002	0.257	.002	2.48	.20	2.81	.28	2.16	.12	1.45	.21	T
12.8	−0.424	0.115	.003	0.261	.003	2.85	.11	2.87	.09	2.83	.13	1.51	.07	C
17.7	−0.284	0.108	.005	0.254	.002	2.20	.37	2.30	.31	2.10	.44	1.67	.27	T
17.9	−0.279	0.111	.005	0.259	.003	2.67	.09	2.77	.08	2.56	.11	1.62	.11	C
24.8	−0.137	0.110	.003	0.252	.002	2.78	.12	2.82	.09	2.74	.15	1.29	.12	C
34.0	0.000	0.099	.005	0.268	.004	2.69	.18	2.80	.13	2.57	.22	1.09	.06	C

NGC 4261 V_h = 2226 km/s r_e = 41 arcsec

r_{int} (")	log r/r_e	Mg_1 (mag)	±	Mg_2 (mag)	±	<Fe> (Å)	±	Fe1 (Å)	±	Fe2 (Å)	±	Hβ (Å)	±	Instr.
0.5	−1.914	0.191	.004	0.353	.006	3.66	.04	3.39	.06	3.94	.03	1.28	.04	T
2.3	−1.251	0.183	.002	0.342	.003	3.36	.06	3.29	.06	3.43	.05	1.18	.03	T
4.7	−0.941	0.175	.002	0.326	.002	3.36	.17	3.21	.10	3.51	.23	1.38	.07	T
5.1	−0.905	0.176	.001	0.329	.001	3.03	.05	3.02	.04	3.04	.07	1.34	.02	C
7.7	−0.726	0.171	.001	0.324	.002	3.08	.07	2.98	.07	3.18	.06	1.46	.06	C
7.9	−0.715	0.168	.001	0.319	.003	3.01	.10	3.00	.15	3.03	.05	1.61	.10	T
10.3	−0.600	0.162	.001	0.314	.002	2.84	.09	2.80	.04	2.89	.13	1.54	.05	C
12.6	−0.512	0.167	.002	0.313	.010	2.88	.29	3.05	.26	2.70	.32	1.54	.09	T
12.9	−0.502	0.160	.001	0.305	.002	2.93	.14	2.88	.09	2.98	.19	1.46	.01	C
16.3	−0.401	0.156	.001	0.299	.004	2.79	.11	2.85	.06	2.74	.15	1.50	.04	C
21.4	−0.282	0.147	.002	0.288	.003	2.87	.16	3.06	.10	2.68	.21	1.35	.02	C
28.2	−0.163	0.142	.003	0.278	.006	2.74	.17	2.64	.18	2.84	.16	1.54	.15	C
37.5	−0.039	0.137	.003	0.268	.005	2.78	.18	2.54	.14	3.02	.22	1.60	.16	C
49.5	0.082	0.115	.007	0.272	.009	2.80	.45	2.73	.48	2.87	.42	1.65	.23	C

For NGC 4472, the gradients seen in our data and those of GES and BT are similar over the radius range in common (see Fig. 6), but our measurements are offset by ≈ 0.4 Å from those of GES and by ≈ 0.9 Å from those of BT. Such offsets are not surprising, since the measured values of both Fe indices are affected by even small differences in spectral resolution. The uncorrected 5270-Å indices measured by BT for NGC 4472, taken with very similar resolution to our TI data, agree well with our raw TI values, but their measurements of the 5335-Å index are about 20 per cent lower than ours and this, together with the lower velocity dispersion they adopted, accounts for the difference.

For the three galaxies in common with Davidge (1992) for which we have measured ⟨Fe⟩, the gradients agree to within the (large) errors, though there is a zero-point offset. The ⟨Fe⟩ index is sensitive to both the resolution used and the velocity dispersion profile of the galaxy, and corrections for these factors were not made by Davidge so, given the large uncertainties, a detailed comparison cannot be made.

Table 4 – *continued*

NGC 4278								V_h = 660 km/s				r_e = 30 arcsec		
r_{int} (")	log r/r_e	Mg_1 (mag)	±	Mg_2 (mag)	±	<Fe> (Å)	±	Fe1 (Å)	±	Fe2 (Å)	±	Hβ (Å)	±	Instr.
0.5	−1.778	0.169	.002	0.314	.001	2.81	.04	2.63	.05	2.99	.02	−.71	.07	T
2.3	−1.115	0.169	.002	0.309	.001	2.56	.04	2.56	.05	2.56	.03	−.28	.05	T
4.7	−0.805	0.162	.001	0.300	.004	2.76	.09	2.63	.13	2.89	.04	0.57	.05	T
5.1	−0.770	0.161	.003	0.299	.003	2.69	.04	2.63	.04	2.76	.04	0.44	.04	C
7.5	−0.602	0.154	.001	0.286	.006	2.56	.08	2.53	.05	2.60	.10	0.58	.01	T
7.7	−0.591	0.151	.004	0.289	.004	2.55	.07	2.56	.06	2.54	.09	0.76	.08	C
10.3	−0.464	0.146	.003	0.277	.004	2.51	.11	2.40	.12	2.61	.10	0.92	.06	C
11.6	−0.413	0.150	.003	0.271	.001	2.42	.21	2.63	.24	2.20	.19	0.95	.12	T
12.9	−0.367	0.138	.003	0.272	.004	2.63	.14	2.71	.09	2.56	.19	1.03	.03	C
16.3	−0.265	0.132	.001	0.259	.002	2.53	.16	2.50	.15	2.56	.18	1.05	.07	C
17.7	−0.229	0.142	.006	0.245	.003	2.49	.01	2.62	.01	2.37	.01	1.28	.07	T
21.4	−0.147	0.127	.002	0.247	.004	2.32	.15	2.31	.12	2.33	.19	0.93	.06	C
28.2	−0.027	0.119	.002	0.238	.005	2.54	.24	2.57	.18	2.51	.29	1.15	.06	C
37.5	0.097	0.112	.004	0.226	.005	2.40	.37	2.44	.45	2.37	.30	0.95	.16	C

NGC 4374								V_h = 1051 km/s				r_e = 53 arcsec		
r_{int} (")	log r/r_e	Mg_1 (mag)	±	Mg_2 (mag)	±	<Fe> (Å)	±	Fe1 (Å)	±	Fe2 (Å)	±	Hβ (Å)	±	Instr.
0.5	−2.025	0.169	.002	0.321	.001	2.93	.06	2.93	.08	2.93	.05	0.88	.09	T
2.3	−1.363	0.165	.001	0.319	.001	2.98	.07	2.99	.05	2.97	.09	1.29	.05	T
4.7	−1.052	0.161	.002	0.314	.001	2.79	.08	2.76	.07	2.83	.08	1.62	.07	T
5.2	−1.017	0.164	.001	0.321	.001	2.86	.05	2.93	.03	2.80	.06	1.34	.02	C
7.0	−0.879	0.154	.003	0.301	.003	2.77	.11	2.79	.08	2.74	.13	1.60	.10	T
7.7	−0.838	0.157	.001	0.311	.001	2.77	.05	2.86	.06	2.67	.03	1.40	.03	C
9.8	−0.733	0.142	.002	0.294	.002	2.56	.15	2.58	.10	2.54	.20	1.32	.09	T
10.3	−0.711	0.149	.001	0.300	.001	2.75	.12	2.74	.06	2.76	.17	1.48	.04	C
12.9	−0.614	0.143	.001	0.294	.001	2.61	.11	2.75	.08	2.48	.14	1.62	.04	C
14.0	−0.578	0.135	.002	0.287	.004	2.71	.13	2.69	.13	2.72	.13	1.31	.09	T
15.5	−0.534	0.140	.002	0.290	.003	2.66	.07	2.76	.09	2.56	.05	1.59	.10	C
18.9	−0.448	0.138	.002	0.285	.002	2.69	.06	2.78	.04	2.61	.08	1.55	.03	C
20.1	−0.421	0.121	.003	0.269	.004	2.65	.17	2.94	.16	2.36	.18	1.28	.13	T
24.0	−0.344	0.128	.002	0.278	.001	2.59	.13	2.79	.09	2.39	.17	1.56	.08	C
30.8	−0.236	0.127	.001	0.271	.003	2.67	.13	2.82	.09	2.51	.16	1.54	.17	C
40.9	−0.113	0.124	.003	0.273	.002	2.66	.17	2.87	.11	2.44	.23	1.57	.20	C
53.9	0.007	0.127	.001	0.269	.005	2.61	.29	2.77	.23	2.45	.35	1.76	.27	C

NGC 4472								V_h = 980 km/s				r_e = 99 arcsec		
r_{int} (")	log r/r_e	Mg_1 (mag)	±	Mg_2 (mag)	±	<Fe> (Å)	±	Fe1 (Å)	±	Fe2 (Å)	±	Hβ (Å)	±	Instr.
0.5	−2.297	0.187	.002	0.354	.002	3.65	.10	3.46	.10	3.84	.09	1.53	.06	T
1.9	−1.717	0.181	.002	0.350	.003	3.41	.08	3.35	.06	3.46	.09	1.57	.06	T
3.3	−1.477	0.175	.002	0.340	.002	3.30	.10	3.33	.08	3.27	.13	1.42	.02	T
4.7	−1.324	0.174	.003	0.337	.002	3.40	.09	3.26	.09	3.54	.09	1.52	.08	T
5.2	−1.280	0.173	.001	0.336	.001	3.49	.04	3.33	.02	3.64	.05	1.36	.04	C
6.1	−1.210	0.172	.002	0.333	.003	3.68	.20	3.48	.17	3.88	.22	1.63	.07	T
7.7	−1.109	0.168	.001	0.330	.001	3.37	.07	3.26	.05	3.47	.08	1.40	.04	C
8.0	−1.093	0.172	.001	0.325	.001	3.21	.15	3.03	.07	3.39	.23	1.48	.11	T
10.3	−0.983	0.167	.001	0.323	.001	3.18	.07	3.12	.10	3.24	.05	1.49	.06	C
11.3	−0.943	0.172	.002	0.321	.002	3.16	.14	2.88	.11	3.43	.18	1.55	.07	T
12.9	−0.885	0.167	.001	0.320	.001	3.17	.08	3.18	.02	3.16	.15	1.40	.04	C
16.3	−0.783	0.164	.001	0.319	.001	3.22	.06	3.02	.04	3.42	.08	1.32	.02	C
16.9	−0.768	0.171	.002	0.321	.003	3.32	.14	3.10	.10	3.54	.19	1.49	.06	T
21.5	−0.663	0.160	.001	0.314	.002	3.26	.07	3.08	.05	3.45	.09	1.44	.02	C
23.9	−0.617	0.167	.002	0.321	.003	3.28	.17	2.92	.17	3.64	.17	1.13	.12	T
28.3	−0.544	0.162	.001	0.310	.002	3.27	.12	3.03	.09	3.52	.15	1.38	.04	C
37.7	−0.419	0.159	.001	0.307	.003	3.08	.17	2.93	.07	3.23	.27	1.43	.09	C
49.7	−0.299	0.155	.001	0.308	.006	2.77	.10	2.81	.15	2.72	.05	1.27	.12	C

3.4 Gradients in Hβ and the effect of Hβ emission

Some caution is needed in the interpretation of the Hβ measurements, since many of the galaxies we observed have Hβ emission. We detect emission of both Hβ and [O III] in NGC 315, 741, 3665, 4261, 4278, 4374, 4486, 4636 and possibly NGC 3379, either directly or after subtracting a template galaxy spectrum. BT found very weak emission in NGC 4472. It would be dangerous to assume that any of the galaxies observed here are without these emission lines. The [O III]/Hβ line ratio suggests that the emission is LINER-like (as is commonly observed in bright ellipticals) rather than

Table 4 – *continued*

NGC 4486						V_h = 1294 km/s						r_e = 95 arcsec		
r_{int} (″)	log r/r_e	Mg_1 (mag)	±	Mg_2 (mag)	±	<Fe> (Å)	±	Fe1 (Å)	±	Fe2 (Å)	±	Hβ (Å)	±	Instr.
0.5	−2.279	0.177	.004	0.277	.007	2.18	.11	2.33	.11	2.03	.12	−3.82	.31	T
1.9	−1.699	0.206	.001	0.349	.005	2.81	.18	2.87	.13	2.75	.22	−.99	.25	T
3.3	−1.459	0.204	.003	0.358	.002	3.07	.18	3.31	.11	2.83	.25	0.41	.14	T
4.7	−1.306	0.204	.003	0.357	.002	3.20	.20	3.23	.18	3.16	.21	0.79	.14	T
5.2	−1.262	0.199	.001	0.356	.001	3.05	.03	3.03	.03	3.07	.04	0.58	.08	C
6.1	−1.192	0.203	.002	0.359	.002	3.35	.20	3.29	.16	3.41	.25	1.01	.21	T
7.7	−1.091	0.197	.001	0.352	.001	3.10	.04	3.03	.02	3.18	.06	0.76	.03	C
8.0	−1.075	0.200	.002	0.354	.002	3.39	.16	3.06	.14	3.71	.19	0.80	.10	T
10.3	−0.965	0.191	.001	0.346	.001	2.98	.07	2.93	.06	3.04	.08	0.84	.05	C
11.3	−0.925	0.194	.002	0.338	.003	3.36	.15	3.10	.11	3.62	.18	1.19	.06	T
12.9	−0.867	0.186	.001	0.339	.001	3.00	.08	2.86	.07	3.13	.10	0.87	.04	C
15.5	−0.787	0.182	.002	0.337	.001	3.06	.06	2.91	.03	3.21	.09	0.98	.04	C
16.8	−0.752	0.178	.002	0.325	.003	3.18	.15	3.32	.15	3.04	.15	1.01	.09	T
18.9	−0.701	0.177	.001	0.327	.001	2.93	.04	2.91	.02	2.95	.07	1.00	.07	C
23.2	−0.612	0.172	.002	0.320	.001	2.95	.06	2.84	.06	2.90	.06	1.14	.09	C
23.9	−0.599	0.169	.003	0.311	.004	3.15	.23	3.12	.16	3.17	.30	1.00	.14	T
27.5	−0.538	0.164	.002	0.315	.003	2.83	.10	2.76	.09	2.89	.11	1.14	.11	C
32.6	−0.465	0.162	.001	0.312	.004	2.60	.13	2.62	.04	2.59	.22	1.15	.12	C
33.1	−0.458	0.150	.003	0.289	.004	2.48	.24	2.66	.21	2.29	.26	1.38	.11	T
39.5	−0.381	0.157	.002	0.302	.005	2.78	.09	2.76	.06	2.80	.13	1.14	.08	C
48.0	−0.296	0.153	.004	0.295	.005	2.68	.19	2.65	.07	2.71	.30	1.15	.04	C

NGC 4636						V_h = 913 km/s						r_e = 67 arcsec		
r_{int} (″)	log r/r_e	Mg_1 (mag)	±	Mg_2 (mag)	±	<Fe> (Å)	±	Fe1 (Å)	±	Fe2 (Å)	±	Hβ (Å)	±	Instr.
0.5	−2.127	0.168	.001	0.332	.003	3.04	.09	3.11	.08	2.97	.09	0.98	.03	T
2.3	−1.464	0.172	.001	0.333	.003	2.88	.10	2.85	.08	2.91	.12	0.93	.12	T
4.7	−1.154	0.161	.002	0.324	.002	2.89	.12	2.89	.09	2.90	.14	1.01	.08	T
5.2	−1.110	0.166	.001	0.323	.002	3.07	.05	3.03	.05	3.12	.05	1.26	.05	C
7.0	−0.981	0.154	.002	0.305	.003	2.76	.11	2.66	.10	2.86	.13	1.21	.13	T
7.7	−0.940	0.159	.001	0.309	.002	2.90	.09	2.84	.04	2.96	.15	1.41	.07	C
10.3	−0.813	0.150	.002	0.299	.001	2.97	.11	2.90	.06	3.03	.16	1.50	.03	C
10.3	−0.813	0.148	.003	0.298	.003	2.86	.13	2.70	.11	3.01	.14	1.17	.09	T
12.9	−0.715	0.148	.001	0.292	.005	2.93	.06	2.93	.06	2.94	.06	1.58	.06	C
15.0	−0.650	0.135	.005	0.294	.006	2.69	.23	2.69	.21	2.70	.24	1.27	.17	T
15.5	−0.636	0.146	.001	0.281	.001	2.80	.09	2.75	.06	2.85	.12	1.61	.07	C
18.9	−0.550	0.139	.002	0.280	.004	2.77	.15	2.59	.13	2.95	.18	1.55	.09	C
24.0	−0.446	0.133	.002	0.270	.001	2.72	.09	2.74	.09	2.69	.09	1.67	.17	C
30.8	−0.338	0.128	.002	0.262	.003	2.55	.10	2.44	.05	2.67	.15	1.65	.14	C
41.0	−0.213	0 120	.003	0.251	.004	2.78	.19	2.60	.13	2.97	.25	1.80	.21	C
53.9	−0.094	0.121	.004	0.241	.004	3.16	.33	2.59	.43	3.73	.23	1.46	.27	C

NGC 4839						V_h = 7213 km/s		r_e = 42 arcsec	
r_{int} (″)	log r/r_e	Mg_1 (mag)	±	Mg_2 (mag)	±	Hβ (Å)	±	Instr.	
5.1	−0.916	0.148	.001	0.299	.002	1.28	.08	C	
8.5	−0.694	0.135	.002	0.286	.004	1.35	.03	C	
12.8	−0.516	0.127	.003	0.281	.003	1.15	.07	C	
18.0	−0.368	0.112	.004	0.261	.004	1.32	.10	C	
24.8	−0.229	0.088	.004	0.255	.010	1.17	.24	C	
34.1	−0.090	0.100	.005	0.256	.007	1.59	.25	C	

from H II regions. DB selected optically luminous, weak radio-emitting ellipticals for kinematic study, which suggests that this sample may be biased towards emission-line objects. In any case, a large fraction of elliptical galaxies have weak emission lines in their nuclei and sometimes further out. Phillips et al. (1986) detected emission lines of N II λ6584 Å in 55–60 per cent of a sample of optically selected elliptical galaxies. Caldwell (1984) detected the O II λ3727-Å line in 40 per cent of his sample. In many galaxies, therefore, the true equivalent width of the Balmer absorption line, especially near the nucleus, will be larger than indicated by the measured Hβ line strength. If the Hβ emission becomes weaker outside the centre, as is usually the case, this will also produce a spurious increase in the apparent Hβ absorption strength. Gradients in the Hβ index can only be interpreted in terms of stellar populations if the effects of emission lines are completely understood.

For the four galaxies in common with Davidge (1992), the measured Hβ gradients agree on average to within the (rather large) errors.

Table 4 – *continued*

NGC 7626						V_h = 3328 km/s						r_e = 34 arcsec		
r_{int} (")	log r/r_e	Mg_1 (mag)	±	Mg_2 (mag)	±	<Fe> (Å)	±	Fe1 (Å)	±	Fe2 (Å)	±	Hβ (Å)	±	Instr.
0.5	−1.833	0.193	.001	0.358	.001	3.34	.06	3.25	.07	3.43	.06	1.15	.02	T
1.9	−1.253	0.188	.001	0.347	.001	3.20	.04	3.13	.03	3.26	.04	1.32	.01	T
3.3	−1.013	0.175	.002	0.328	.001	3.14	.02	3.10	.01	3.17	.05	1.34	.08	T
5.1	−0.824	0.156	.005	0.314	.005	2.99	.03	2.92	.05	3.06	.02	1.23	.06	C
5.2	−0.815	0.164	.001	0.312	.006	3.07	.05	3.22	.04	2.92	.05	1.40	.16	T
7.5	−0.656	0.152	.004	0.303	.002	3.01	.06	3.07	.09	2.94	.02	1.52	.14	T
7.7	−0.645	0.148	.003	0.303	.002	2.89	.16	2.94	.13	2.83	.19	1.17	.06	C
10.3	−0.519	0.152	.001	0.293	.004	3.20	.06	3.39	.03	3.01	.09	1.49	.12	T
11.1	−0.486	0.141	.002	0.294	.003	2.91	.08	2.92	.07	2.91	.10	1.22	.07	C
14.0	−0.385	0.136	.001	0.284	.001	2.76	.34	3.16	.15	2.37	.53	1.23	.12	T
15.4	−0.344	0.140	.003	0.292	.002	3.11	.20	3.02	.15	3.21	.26	1.22	.13	C
18.7	−0.260	0.137	.001	0.281	.005	2.78	.22	2.44	.32	3.11	.11	1.48	.05	T
20.5	−0.220	0.124	.001	0.273	.003	2.94	.16	2.87	.12	3.01	.19	1.19	.04	C
27.3	−0.095	0.121	.006	0.257	.009	2.48	.18	2.46	.08	2.50	.28	1.09	.18	C
37.4	0.041	0.122	.009	0.265	.015	2.43	.55	2.67	.39	2.18	.72	0.68	.39	C

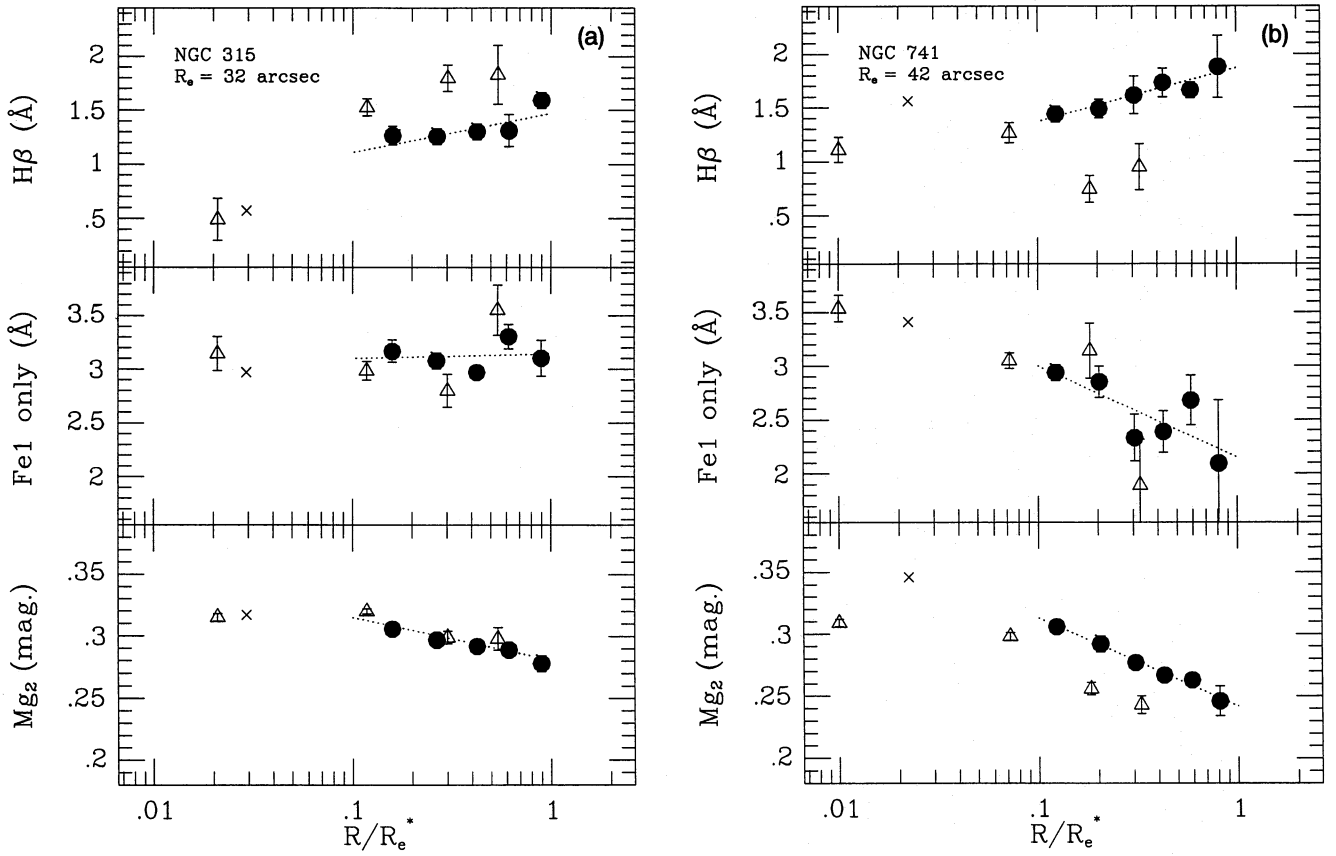

Figure 5. Final corrected Hβ, ⟨Fe⟩ and Mg_2 indices for each galaxy, versus r/r_e^*. Cryocam data are indicated with filled circles, while TI indices are shown by open triangles. The crosses are central values from Faber, Gonzalez and collaborators. Also drawn are the best-fitting linear relations (as dotted lines) from which the gradients have been derived (see Table 5).

3.5 Consistency with other observers

Line-strength measurements are now available from several studies using a variety of instrumental configurations and detectors. For example, Couture & Hardy (1988) and GES used photon-counting detectors, while we, BT and Davidge used CCDs. The spectral resolution used varies from 11–12 Å for low-resolution, high-efficiency spectrographs like the KPNO Cryocam (which can measure line strengths at reasonable signal-to-noise ratio in the faint outer parts of galaxies) to 1–2 Å for the observations of NGC 5813 described by Efstathiou & Gorgas (1985). It is therefore interesting to see to what extent these diverse observations yield consistent results.

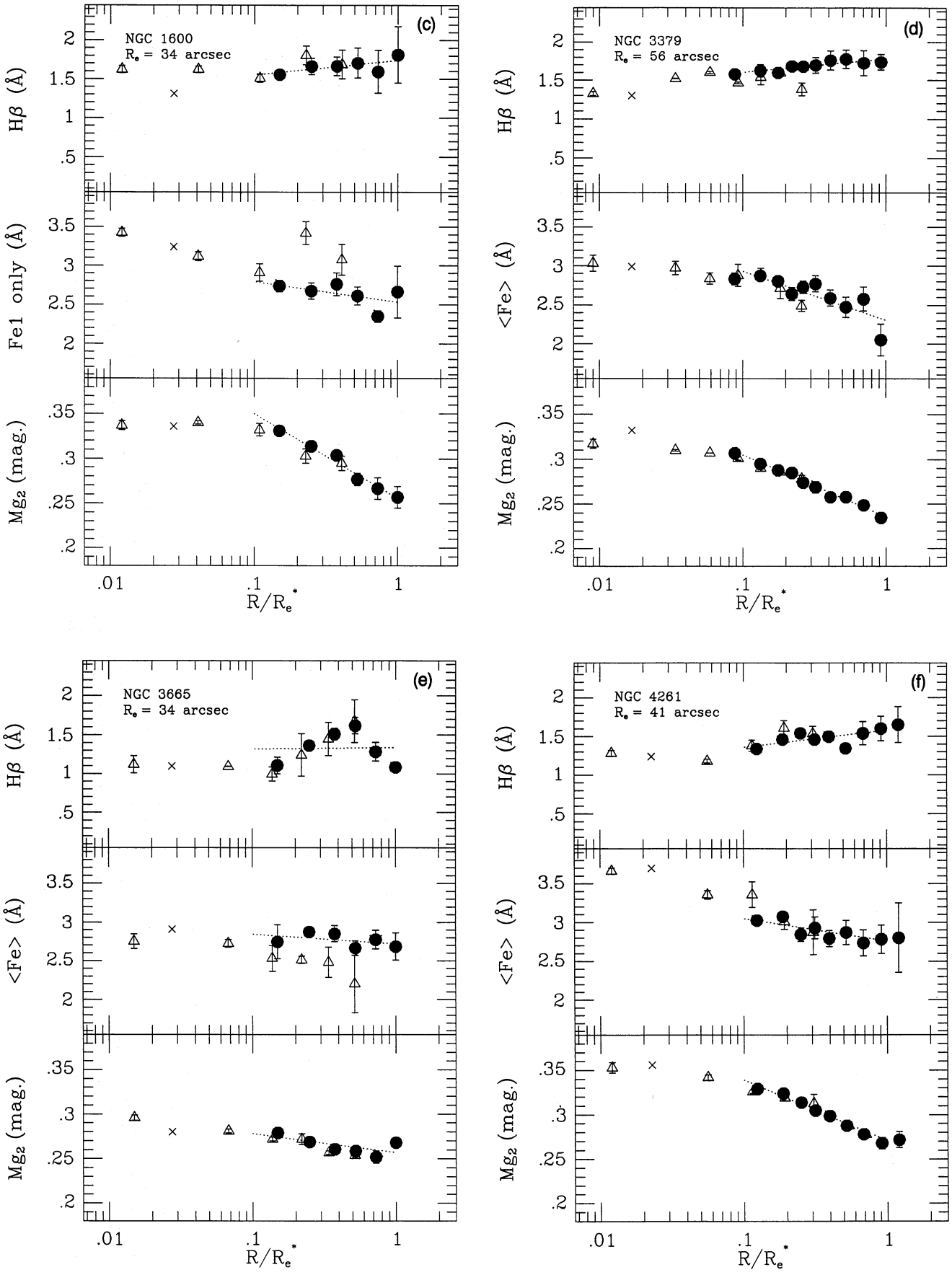

Figure 5 – *continued*

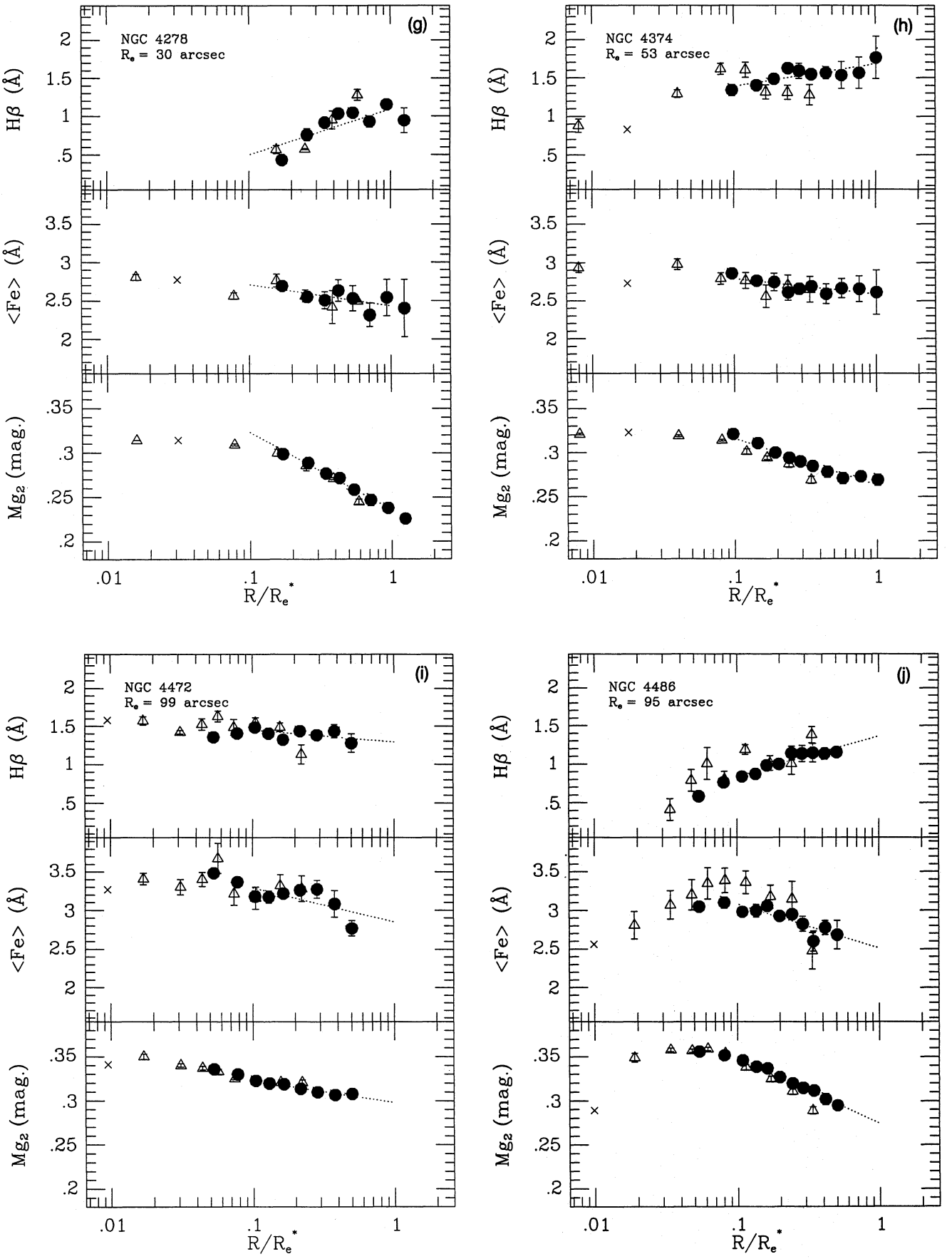

Figure 5 – *continued*

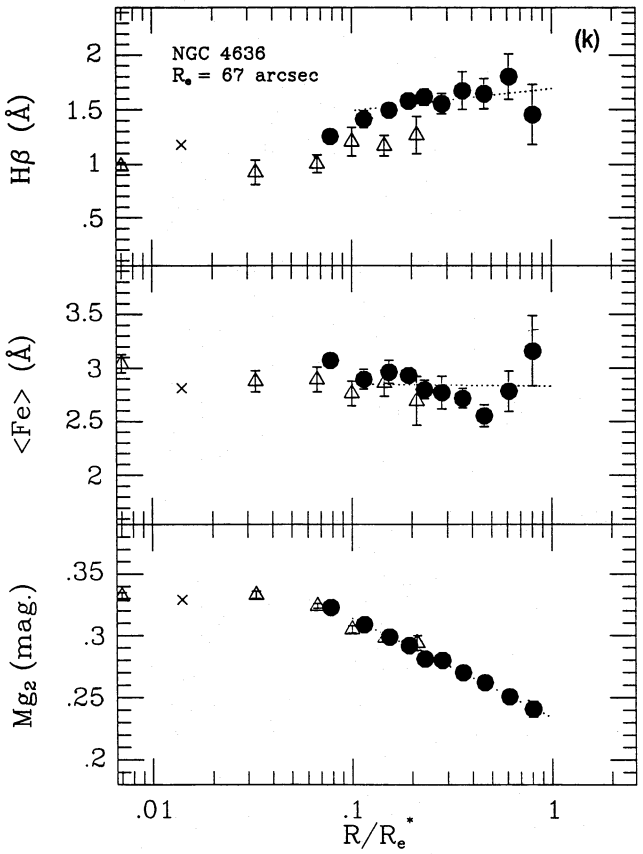

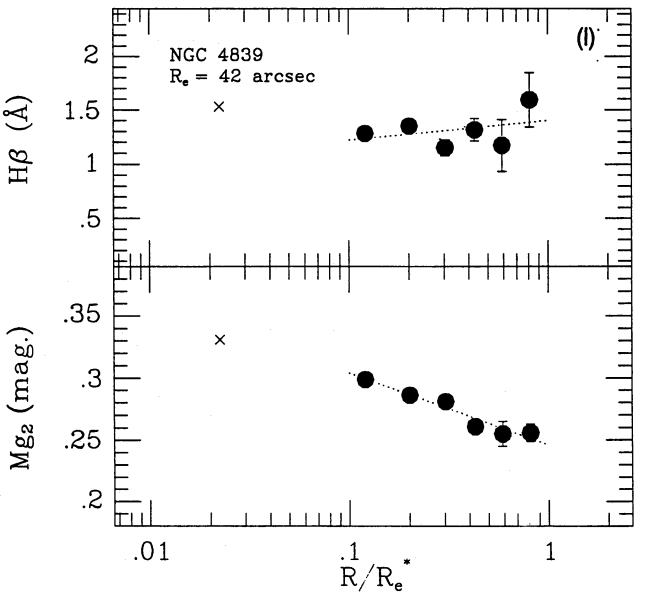

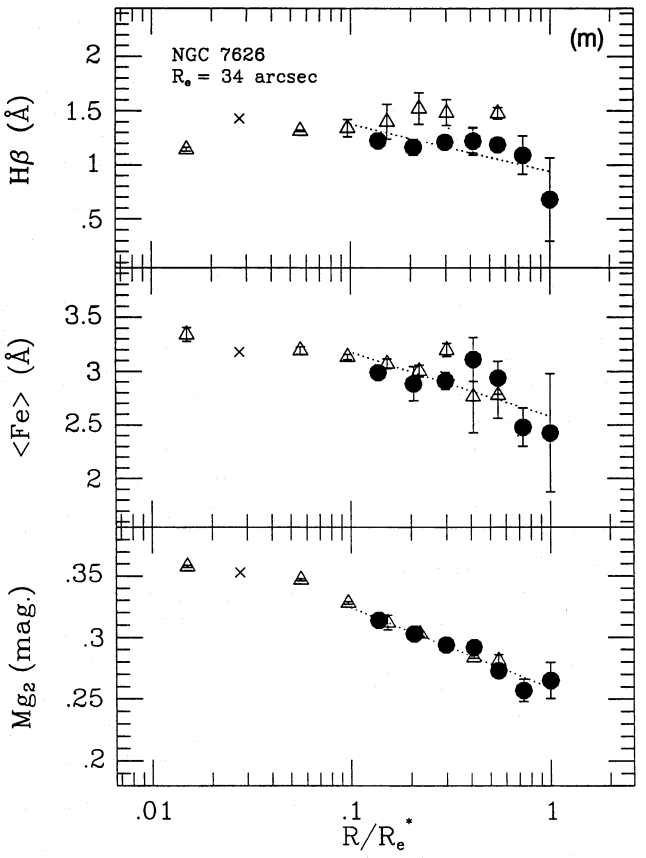

Figure 5 – *continued*

Table 5. Final line-strength gradients and other global parameters.

Galaxy	M_B	Range (r/r_e)	Mg_2 (mag) Slope ±	Mg_2 (mag) Int ±	Mg_1 (mag) Slope ±	Mg_1 (mag) Int ±	<Fe> (Å) Slope ±	<Fe> (Å) Int ±	Hβ (Å) Slope ±	Hβ (Å) Int ±	σ (km s^{-1}) Slope ±	Δ Hβ (Å) Central 0.5 r_e
NGC 315	−23.1	0.12–0.9	−0.031	0.282	−0.040	0.125			0.355	1.622		−1.03
			.007	.003	.011	.005			.423	.195		−0.12
NGC 741	−22.8	0.08–0.8	−0.058	0.240	−0.046	0.110			0.757	1.814		−0.42
			.023	.013	.013	.007			.510	.283		−0.26
NGC 1600	−22.9	0.11–1.0	−0.088	0.257	−0.058	0.120			0.114	1.733	−0.137	0.13
			.009	.004	.007	.003			.125	.061	0.090	0.12
NGC 3379	−20.6	0.06–1.0	−0.065	0.238	−0.049	0.115	−0.592	2.315	0.247	1.777	−0.205	−0.19
			.003	.002	.004	.003	.114	.076	.077	.051	0.009	0.04
NGC 3665	−21.6	0.14–1.0	−0.022	0.254	−0.037	0.101	−0.087	2.608	0.119	1.420		−0.42
			.010	.005	.004	.002	.307	.147	.299	.143		−0.37
NGC 4261	−21.7	0.11–1.2	−0.068	0.271	−0.056	0.130	−0.297	2.758	0.163	1.579	−0.121	−0.19
			.005	.002	.005	.003	.068	.036	.094	.049	0.029	−0.11
NGC 4278	−19.2	0.16–1.3	−0.088	0.234	−0.057	0.120	−0.254	2.425	0.688	1.148	−0.098	−2.23
			.005	.002	.005	.002	.106	.045	.210	.089	0.012	−1.04
NGC 4374	−21.5	0.09–1.0	−0.050	0.262	−0.040	0.118	−0.173	2.590	0.245	1.625	−0.115	−0.63
			.006	.004	.006	.003	.062	.038	.120	.073	0.023	−0.08
NGC 4472	−22.4	0.03–0.5	−0.028	0.297	−0.017	0.153	−0.499	2.833	−0.199	1.248	−0.071	0.06
			.003	.002	.003	.002	.136	.119	.104	.091	0.014	0.08
NGC 4486	−22.1	0.06–0.5	−0.076	0.270	−0.062	0.132	−0.810	2.394	0.428	1.349	−0.089	−2.47
			.005	.004	.003	.003	.154	.120	.114	.088	0.009	−0.54
NGC 4636	−20.6	0.07–0.8	−0.077	0.236	−0.045	0.113	−0.087	2.788	0.435	1.749	−0.050	−0.52
			.003	.002	.003	.002	.159	.112	.146	.102	0.019	−0.19
NGC 4839	−23.2	0.12–0.8	−0.058	0.246	−0.070	0.086			0.181	1.396		−0.26
			.008	.004	.012	.007			.246	.134		−0.30
NGC 7626	−22.1	0.10–1.1	−0.063	0.262	−0.048	0.120	−0.622	2.611	−0.495	1.028	−0.040	−0.32
			.005	.003	.005	.003	.189	.096	.210	.106	0.024	−0.21

First of all, there are few absorption lines that are strong enough to be measured with any accuracy at all at $1r_e$. In the region we are considering here (roughly 4500–6000 Å), Mg_2 and ⟨Fe⟩ are the main indices that are both measurable and likely to yield useful information (Hβ is severely contaminated by emission in many ellipticals, as noted above, and, while Na D is strong in the nuclei of many galaxies, it becomes rapidly weaker towards large radii).

It is reassuring, therefore, that the Mg_2 gradients measured by different studies are generally in agreement. It is clear that Mg_2 is a robust index, and that the results obtained by different authors do not appear to depend on the detectors or resolution used. The ⟨Fe⟩ index is less robust, being affected even by small changes in velocity dispersion or spectral resolution but, nevertheless, ⟨Fe⟩ gradients measured by different authors generally appear to agree to within the quoted errors.

3.6 Global correlations

We have investigated whether the line-strength gradients for this sample correlate with other global galaxy parameters. These include colour gradients in $B-R$ and $U-R$, central Mg_2, central velocity dispersion, X-ray luminosity, central escape velocity, (V/σ), $(V/\sigma)^*$, V_{rot}, total blue luminosity, ellipticity and radio continuum flux at 5 GHz. The parameters were obtained from Table 2, Birkinshaw & Davies (1985) and PDIDC.

None of the parameters correlates very well with the gradient in any of the line-strength indices, although with a small sample, substantial errors in the ⟨Fe⟩ and Hβ gradients and a relatively small range in luminosity, velocity dispersion and ellipticity represented in the sample, this is perhaps to be expected. Furthermore, we note that PDIDC found that colour gradients do not correlate well with other global parameters.

The best two correlations are worth further mention. The correlation of the gradient in Mg_2 with the gradient in $U-R$ has a correlation coefficient of 0.71. $U-R$ is the colour gradient with the smallest uncertainty from observations, while Mg_2 is the best-determined line-strength index. The fact that this correlation is the best of all correlations between line-strength gradients and colour gradients suggests that better data might reveal a very good correspond-

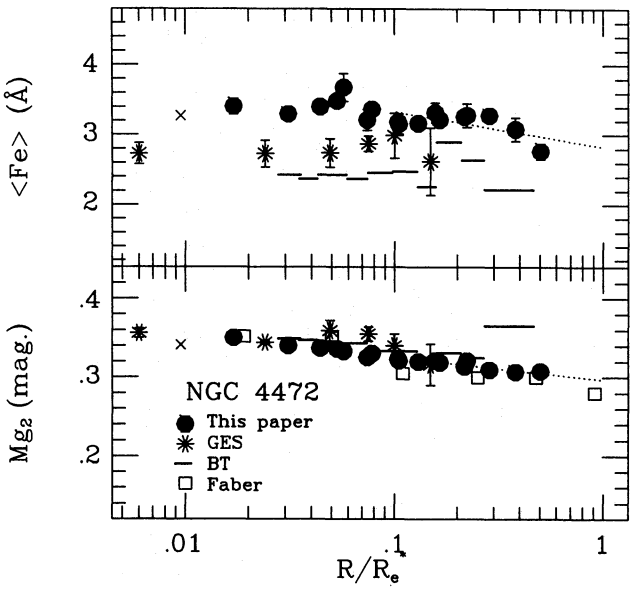

Figure 6. Comparison of the indices of NGC 4472 with those derived by other authors. For our data, symbols are as in Fig. 5; data from other authors are represented by open squares (Faber 1977), stars (GES) and bars (BT).

ence. The correlations between the gradient in Hβ and the gradients in $B-R$ and $U-R$ have correlation coefficients of -0.71 and -0.68. We suggest later that the Hβ gradient arises mainly from the *decreasing* strength of emission lines with increasing radius. Since the presence of gas usually coincides with the presence of dust, larger colour gradients might be expected. The galaxy in this sample with the largest colour gradient is NGC 4278, an object that is known to be dusty (Ebneter & Balick 1985).

4 ABUNDANCES AND ABUNDANCE GRADIENTS

Using the calibration by Mould (1978), and assuming that radial change in Mg_2 is due to metallicity changes alone, we find that the average gradient in Mg_2 corresponds to a gradient in [Fe/H], Δ[Fe/H]/$\Delta \log r$, of -0.23 ± 0.09. For $\langle$Fe$\rangle$, we adopt the empirical relation derived by Faber et al. (1985) to derive a gradient of -0.21 ± 0.10 in [Fe/H]. These values are similar to the values of Δ[Fe/H]/$\Delta \log r$ of -0.22 ± 0.10 derived from the Mg_2 index by GES and -0.25 derived by Couture & Hardy (1988), both also using Mould's (1978) relation between Mg_2 and [Fe/H]. These values are remarkably consistent and, if the interpretation is correct, imply that abundance gradients in ellipticals are rather shallow. This interpretation is not unique; the conversion from line-strength gradients to abundance gradients is not straightforward. At each position in the galaxy, we measure lines that arise from a superposition of all the components of the stellar population sampled along the line of sight and broadened by the velocity dispersion. The population components may be neither coeval nor of uniform metallicity. Furthermore, age and metallicity are hard to disentangle, since the observable consequences of a change in age for an integrated stellar population can be reproduced almost entirely by a change in metallicity (e.g. Tinsley & Gunn 1976). Here we explore the relationships between the line strengths and gradients that we have measured, and their correlations with other properties of elliptical galaxies, in an attempt to gain a better understanding of the stellar populations and possibly to separate the effects of age and metallicity.

4.1 Line-strength gradients and colour gradients

PDIDC determined colour gradients in $U-R$ and $B-R$ for 39 elliptical galaxies. The average colour gradients corresponded to a decrease of -0.20 in [Fe/H] per decade in radius. Similarly, Franx, Illingworth & Heckman (1989) measured colour gradients for a sample of 17 southern ellipticals and found an average gradient of -0.22. These values agree very well with the average values obtained from both Mg_2 and $\langle$Fe$\rangle$ in this paper. This agreement is encouraging, as it demonstrates that both colours and line strengths, when interpreted as metallicity effects, give a consistent picture of small mean abundance gradients.

We have explored the correlation between *local* colour and line strength in our sample. In Fig. 7 we show $B-R$ versus Mg_2. (For three galaxies, it was necessary to revise the absolute calibration from PDIDC as indicated in the figure caption.) The correlation between colour and line strength is consistent with the scatter being entirely due to the measurement errors. Similarly, the scatter in the relations between Mg_2 and $U-R$, and $\langle$Fe$\rangle$ and colour, is consistent with the measurement errors, but the uncertainties in these quantities are substantially larger than those in Fig. 7. Also plotted are the fit to the values from the nuclei of elliptical galaxies from Davies et al. (1987) and Burstein et al. (1987) (solid line), and the expected relation between $B-R$ and Mg_2 for stellar populations with a solar [Mg/Fe] ratio and ages of 20 and 12 Gyr from Peletier (1989, dotted and dot–dashed lines respectively). Note that the points lie above the line describing the relation for the nuclei.

The correlation between line strength and colour shows that colour gradients are not generated by dust distributed throughout elliptical galaxies, as has been suggested by e.g. Witt, Thronson & Capuano (1992). At the most, the scatter in $B-R$ at a fixed Mg_2 (0.03 mag) indicates that A_V is no more than 0.06 mag, so that dust extinction cannot be responsible for the colour gradients.

4.2 Relations between line indices

4.2.1 $\langle$Fe$\rangle$ versus Mg_2

In Fig. 8 we plot $\langle$Fe$\rangle$ versus Mg_2 for the data reported here. The solid line indicates the mean relation followed by the nuclei of 170 elliptical galaxies (from BFGK). Two models are plotted, showing the expected relation for stellar populations with solar values of [Mg/Fe], spanning the range of [Fe/H] from 0.25 to 2.5 times the solar value, and with ages of 12 and 20 Gyr, taken from Peletier (1989). These models are in good agreement with those of Worthey as given in FWG.

There is a tight relation between $\langle$Fe$\rangle$ and Mg_2, with no more scatter than expected from the small uncertainties. The relation for the nuclei of galaxies has a shallower slope than the gradients within the galaxies, confirming the results of

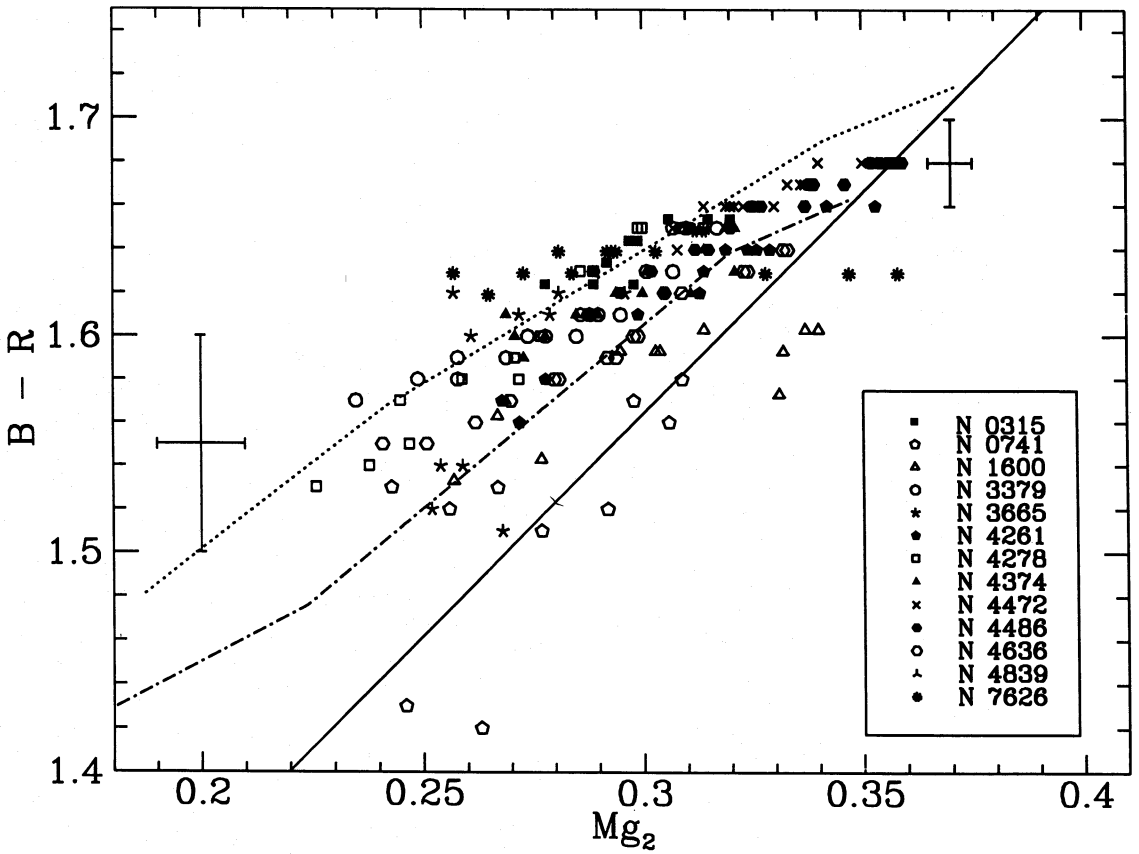

Figure 7. Local $B-R$ colour versus Mg_2 for the sample. Also drawn are the best-fitting line to the results for the nuclei of early-type galaxies (from Burstein et al. 1987; Davies et al. 1987 – solid line) and some models for old stellar populations of ages 20 Gyr (dotted line) and 12 Gyr (dot–dashed line) from Peletier (1989). The local colours are from Peletier et al. (1990). The error bars indicate typical random errors in the centre (right-hand side) and in the outer parts (left-hand side) of the galaxies. Errors in the absolute zero-point for each galaxy could be as high as 0.05 mag. The zero-points for NGC 315, 7626 and 1600 were recalibrated by converting the $B-V$ colours of Burstein et al. (1987) to $B-R$, as in Peletier et al. (1990).

GES and FWG. For the nuclei, $\delta\langle\mathrm{Fe}\rangle/\delta\mathrm{Mg}_2 \approx 3$ while, for the gradients, $\delta\mathrm{Mg}_2/\delta\langle\mathrm{Fe}\rangle \approx 8$. At low values of Mg_2 and $\langle\mathrm{Fe}\rangle$, the points from the outer parts of ellipticals almost overlap the globular cluster measurements of BFGK with a similar slope.

Beyond the range of our data, the model lines intersect the position of elliptical galaxy nuclei at low values of $\langle\mathrm{Fe}\rangle$ and Mg_2. FWG pointed out that the models provide a satisfactory fit to the compact ellipticals, which typically have metallicities slightly less than solar. However, as FWG also noted, this implies that throughout the giant ellipticals Mg is enhanced with respect to Fe compared with the solar ratio. As the models for 12 and 20 Gyr lie almost on top of each other, the luminous ellipticals cannot be fitted by changing either the age or the metallicity (fixed at a solar distribution). In addition, as the Fe and Mg lines originate in the atmospheres of the same stars, it is hard to think of a systematic error in the stellar mix of the models that could cause an anomaly that would operate only in the regime of the giant ellipticals. The explanation appears to be that the abundance ratio of Mg to Fe is enhanced with respect to that of the solar neighbourhood throughout giant elliptical galaxies (as suggested by Peletier 1989, Matteucci 1992 and FWG). This hypothesis implies that the slope of $\langle\mathrm{Fe}\rangle$ versus Mg_2 within these galaxies is the same as that of the models, while for a given value of Mg_2 the observed $\langle\mathrm{Fe}\rangle$ is too low (as is observed).

Although abundance anomalies are common in our own Galaxy (see e.g. Gilmore, Wyse & Kuijken 1989 for a review), it is very difficult to calculate by how much Mg is enhanced with respect to Fe, since no stellar evolutionary tracks are available to calibrate this effect. FWG discussed the ways in which [Mg/Fe] can be varied. Most of the Mg originates in the Type II supernova explosions of massive stars, whereas Fe is mostly made in the Type Ia supernovae which have mass-transferring binaries as progenitors. There is a lag between the early production of Mg and the later production of Fe, so the star formation history of a galaxy will influence the [Mg/Fe] ratio. In principle, the effect observed could be generated by a deficit of $\langle\mathrm{Fe}\rangle$ compared to Mg_2; because $\langle\mathrm{Fe}\rangle$ arises in longer lived low-mass stars, however, the mechanisms for production of such a deficit are harder to envisage. The selective loss of $\langle\mathrm{Fe}\rangle$ seems unlikely (although it might be possible via the late onset of a galactic wind); one possibility is a lower binary fraction in ellipticals, which would reduce the number of iron-generating Type Ia supernovae. The enhancement of Mg could be produced more straightforwardly if giant ellipticals experienced more generations of massive star formation prior to significant Fe pro-

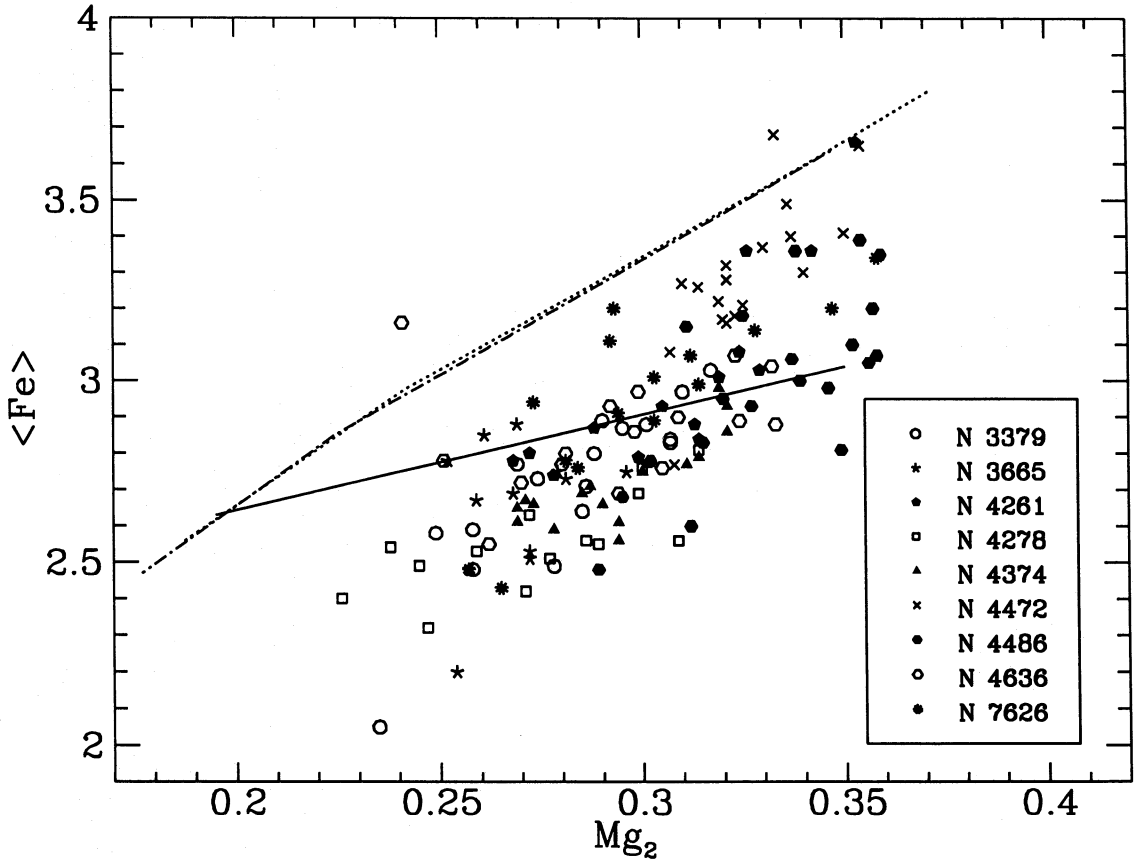

Figure 8. The relationship between local Mg_2 and $\langle Fe \rangle$ for our galaxies. Also plotted are the best fit to the nuclei of 170 elliptical galaxies (from Burstein et al. 1984, solid line), and two models for old stellar populations with solar ratios of [Mg/Fe] and ages of 20 Gyr (dotted line) and 12 Gyr (dot–dashed line) from Peletier (1989).

duction, or if the initial mass function were more skewed towards massive stars than the Salpeter function used in the models.

An alternative to the enhanced-Mg/Fe hypothesis has been suggested by Sadler (1992). Drawing on a survey of the M-giant population in Baade's window, she suggests that, *if* M-giant stars later than M2 were to contribute 10 per cent of the *V*-band light in ellipticals, the apparent abundance anomaly could be explained by stars with solar abundance ratios. This possibility is not consistent with the fraction of M giants later than M2 (1–2 per cent) derived in the population syntheses of Pickles (1985) or Peletier (1989). In addition, such a large fraction of *V*-band light from M giants would produce $V-K$ colours at least 0.2 mag too red for the galaxies. Since metal-rich giants are bluer for a given line strength than are nearby field giants (Frogel & Whitford 1987), the latter problem might be not so serious.

4.2.2 *Hβ versus Mg_2*

In Fig. 9, Hβ is plotted as a function of Mg_2. Also shown are Worthey's models, from FWG, for stellar populations of ages 6 and 18 Gyr. The older model describes the upper envelope of the distribution of points quite well. Note that most of the galaxies observed exhibit *increasing* Hβ absorption-line strength with decreasing Mg_2 (or increasing radius). Many of the galaxies observed here exhibit extended Hβ emission, and the increasing absorption-line strength arises as the emission line gets weaker away from the centre. The exception is NGC 4472, which has no emission and shows decreasing values of the Hβ index with increasing radius.

To quantify the amount of Hβ emission, we have calculated for each galaxy the difference between measured Hβ absorption and the Hβ absorption expected at a given value of Mg_2 for a quiescent galaxy of age 18 Gyr, as represented by the model of Worthey given in FWG. (The calibration would have been almost the same had we used the line connecting the upper envelope of points in Fig. 9.) For each point, ΔHβ has been calculated with respect to Worthey's relation:

$$\Delta H\beta = H\beta - 1.91 + 1.24 Mg_2.$$

In Table 5 we give the central values of ΔHβ, as well as a luminosity-weighted average value out to one-half of the effective radius.

A decrease in the age of the stellar population (or contamination by a younger population) moves the models to higher values of Hβ absorption. If the upper envelope of points in Fig. 9 represents the stellar population free of the effects of Hβ emission, however, then these data show no evidence for an intermediate-age population of stars.

In cases where emission was present, FWG 'pruned' their spectra of excess Hβ emission based on the presence of the [O III] 5007-Å line, and reported no gradient in Hβ for 28 *cluster* ellipticals. From their flat Hβ profiles, they inferred

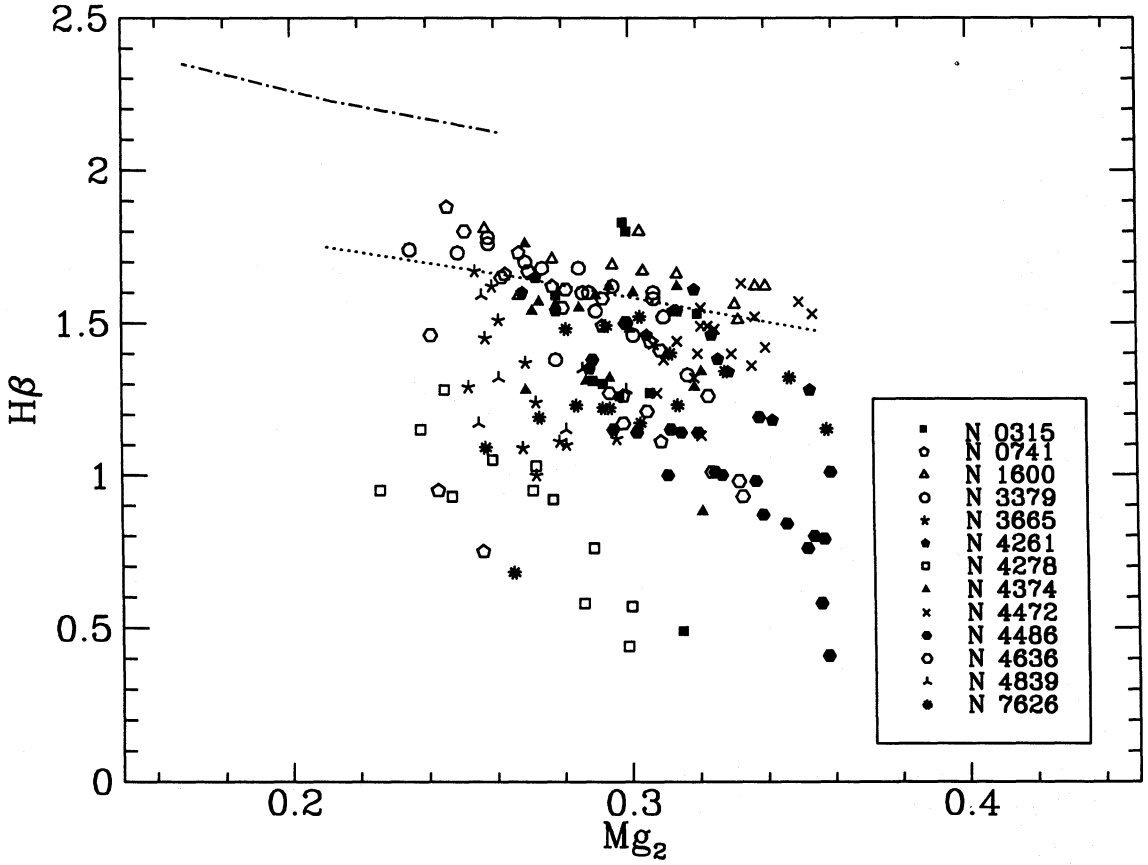

Figure 9. Relation between Hβ and Mg_2 for the galaxies. Here we have also plotted models by Worthey (FWG) for stellar populations of age 18 Gyr (lower values of Hβ) and 6 Gyr.

that the centres of ellipticals might be younger than the envelopes. We have not attempted to correct for nuclear emission, but for our sample of galaxies, originally chosen as (mostly weak) radio sources, it seems more reasonable to invoke a 'standard' old stellar population, with the central Hβ absorption polluted by extended emission, than to infer the presence of an age gradient.

For five of our galaxies, UV fluxes have been tabulated by Burstein et al. (1988). A plot of $1550-V$ colour versus ΔHβ (Fig. 10) shows that the two galaxies with the largest ΔHβ have by far the bluest $1550-V$ colour. We speculate here that the inverse relationship between Mg_2 and $1550-V$ reported by Burstein et al. could be due to the presence of an otherwise undetected blue ionizing nucleus in galaxies with high values of Mg_2. Perhaps both the activity which generates the Hβ emission and the high values of metallicity result from the star formation associated with the formation of a core. The data presented here are consistent with that event being more or less contemporaneous with the formation of the rest of the galaxy, although dating of such an event remains a highly uncertain exercise.

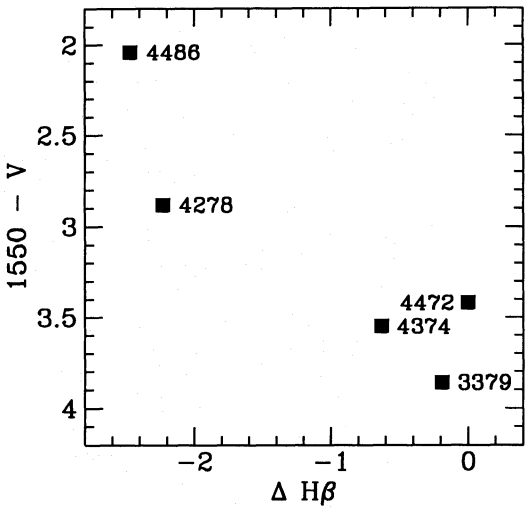

Figure 10. Relation between ΔHβ (see Section 4.2 for a definition) and $1550-V$ from Burstein et al. (1988) for the five galaxies in common. Both galaxies with very blue $1550-V$ colours (NGC 4278 and 4486) also have a large value of ΔHβ.

5 RELATIONSHIPS WITH DYNAMICAL PROPERTIES

5.1 Line strengths and the local escape velocity

Franx & Illingworth (1990) noted that the colour–colour relation between $B-R$ and $U-R$ does not vary significantly from galaxy to galaxy, and they investigated whether the local colour (which they equated with metallicity) within an elliptical might be a function of the local escape velocity. They calculated the internal colour gradient expected on the basis of the correlation between the mean colour and central

velocity dispersion, using models for the potential with and without dark matter. They found that, for their sample of 17 galaxies, within the errors, local colour is the same function of local escape velocity for all of the galaxies.

We can use our measurements of line-strength gradients to investigate this connection more directly. Franx (private communication) has calculated V_{esc} from surface photometry and kinematics for each of the galaxies in the compilation of van der Marel (1991) (Jørgensen, Franx & Kjaergaard 1992) on the basis of axisymmetric, two-integral models (Binney, Davies & Illingworth 1990; van der Marel, Binney & Davies 1990). These escape velocities are determined from separate model fits to the kinematics and photometry of the individual galaxies, rather than from the simple parametrized luminosity laws that were used in Franx & Illingworth (1990). In Fig. 11(a) we plot Mg_2 against this local escape velocity for the galaxies in common with our sample. The correlation is good, a scatter of 0.05 in Mg_2 at fixed V_{esc}, corresponding to a scatter in [Fe/H] of 0.2. While only a limited range of both parameters is explored, the suggestion by Franx & Illingworth (1990) that metallicity is a function of the *local* escape velocity is confirmed, using a more direct indicator of metallicity and a more appropriate calculation of V_{esc} for each galaxy.

In Fig. 11(b) we plot *local* Mg_2 versus *local* velocity dispersion. We have used the correlation between the central values of these parameters (Burstein et al. 1987; Davies et al. 1987) to predict how they should vary together within galaxies. This is shown as the solid line in Fig. 11(b). We note that for a given change in Mg_2 the change in σ is much less than predicted by the relation between the central values. It seems likely that effects of anisotropy and rotation account for the fact that velocity dispersion is a much poorer indicator of metallicity than is V_{esc}.

5.2 Kinematic subcomponents

For four galaxies exhibiting peculiar core kinematics, Bender & Surma (1992) showed that the Mg_2 index exhibits a change of slope at roughly the same radius at which the peculiar core kinematics start to show up. They outlined a picture in which the core stars with anomalous kinematics form from enriched material after the main body of the galaxy has formed.

There are two galaxies in our sample with anomalous core kinematics: NGC 4472 (DB) and NGC 7626 (Jedrzejewski & Schechter 1989). In Fig. 12 we plot Mg_2 and V_{rot} as functions of radius for these galaxies. In NGC 4472 the Mg_2 index continues to rise within the radius where the counter-rotating core is found (about 10 arcsec); however, there is no clear break in the slope. The total increase in Mg_2 within the region of anomalous kinematics is 0.03 mag (about 0.12 in [Fe/H]). In NGC 7626 the increase in Mg_2 is greater, 0.06 mag (about 0.24 in Fe/H]), and in linear radius there is a clear change of slope at the radius where the velocity anomaly in the core starts. In both galaxies, the change in the slope of Mg_2 is small. Fig. 5 shows that gradients in Mg2 persist throughout galaxies, and that typical ellipticals do not have a high-metallicity core residing in a uniform-metallicity halo.

Balcells & Quinn (1990) have suggested that anomalous core kinematics could arise when a smaller, high surface brightness galaxy falls into an elliptical and survives into the centre because of its high binding energy. Since this process is entirely stellar, the population in the anomalous core should correspond to that of a galaxy of lower luminosity. Such galaxies in general have lower central line strengths, although rare examples do have very high central line strengths, for example NGC 4486B and 5846A with $Mg_2 \sim 0.30$. However, *none* of the low-luminosity galaxies in the sample of Faber et al. (1989) reaches values as high as those in the central regions of NGC 4472 and 7626 ($Mg_2 \sim 0.35$). The high metallicity of the anomalous cores rules out the Balcells & Quinn picture of capture of a low-mass, strong-lined galaxy of the type we observe today, and indicates that much of the core light is contributed by stars that formed from enriched material probably generated by the star formation that was associated with the formation of the core itself. However, since Hβ absorption is not enhanced in the two anomalous cores for which we have data, there is no indication that these core stars formed *much* later than the rest of the galaxy.

Statler (1991) has shown that the projected velocity field of triaxial 'perfect ellipsoids' will exhibit anomalous kinematic behaviour a substantial fraction of the time. This hypothesis, that the peculiar core kinematics arise from the varying contributions from the competing families of tube orbits projected on to the sky, is consistent with all the data presented here. However, it is not clear in this picture how the correlation between position and metallicity arises.

6 CONCLUSIONS

(1) We have measured line-strength gradients in Mg_2, $\langle Fe \rangle$ and Hβ for 13 galaxies using two instruments on the KPNO 4-m telescope. The galaxies observed were those used by Davies & Birkinshaw (1988) to investigate the kinematics of (mostly low-power) radio-loud elliptical galaxies. The metal-line strengths are consistent with an average abundance gradient of $\Delta[Fe/H]/\Delta \log r = -0.2 \pm 0.1$, or a reduction in mean metallicity of the stellar population of 40 per cent over a factor of 10 in radius. Both line strengths and colours, when interpreted in terms of abundance gradients, give a consistent picture of small mean abundance gradients. These shallow gradients present a significant challenge to current theories of galaxy formation. Dissipative models (Larson 1976; Carlberg 1984) produce gradients that are steeper than those measured in giant ellipticals. On the other hand, models of the formation of ellipticals that rely on stellar interactions alone, such as dissipationless hierarchical merging, have no mechanism for the generation of metallicity gradients. White (1980) showed that an *existing* gradient would be diluted by about a factor of 2 over three merger events. Together, these considerations support the hypothesis that giant ellipticals form by predominantly stellar mergers, and that the line-strength gradients originate in their lower mass progenitors which formed predominantly by dissipative collapse. Recently, Bender, Burstein & Faber (1992) have noted that the *global* properties of dynamically hot galaxies are also consistent with the degree of dissipation decreasing as mass increases. They regard this sequence as a 'gas/stellar' continuum in which galaxies form from progenitors with lower gas-to-star ratios as the total mass increases.

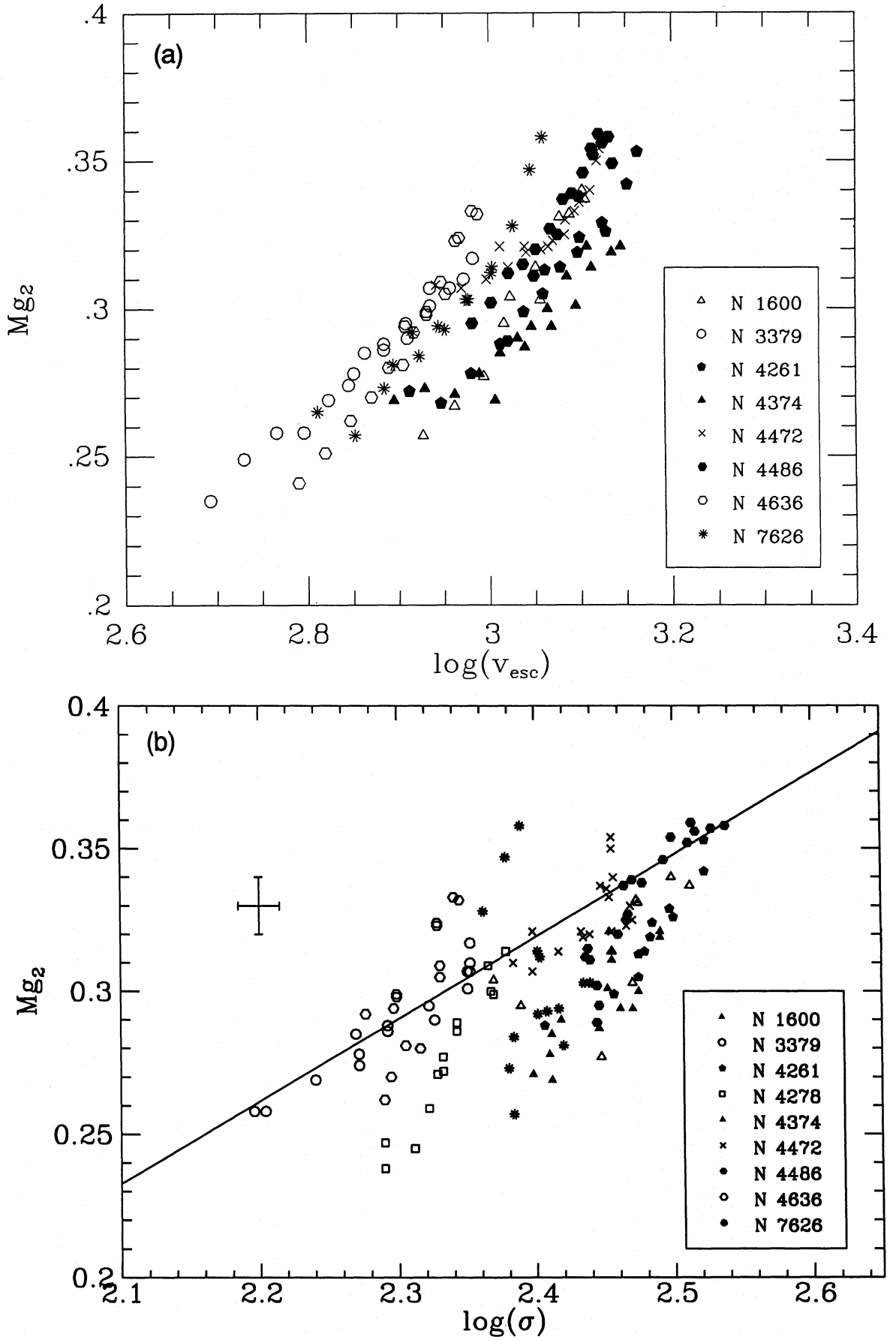

Figure 11. (a) Mg_2 plotted against local escape velocity, $\log V_{esc}$, for those galaxies in common with van der Marel (1991). The escape velocities were provided by M. Franx and are calculated by using the observed kinematics and photometry and fitting a two-integral, axisymmetric model. (b) Local Mg_2 as a function of $\log(\sigma)$ for nine galaxies for which good velocity dispersion profiles were available (all except NGC 315, 741, 3665 and 4839). For NGC 1600 and 7626, the dispersion profiles were taken from Jedrzejewski & Schechter (1989); the remainder were from DB. The solid line is the relationship for elliptical galaxy nuclei taken from Burstein et al. (1987) and Davies et al. (1987).

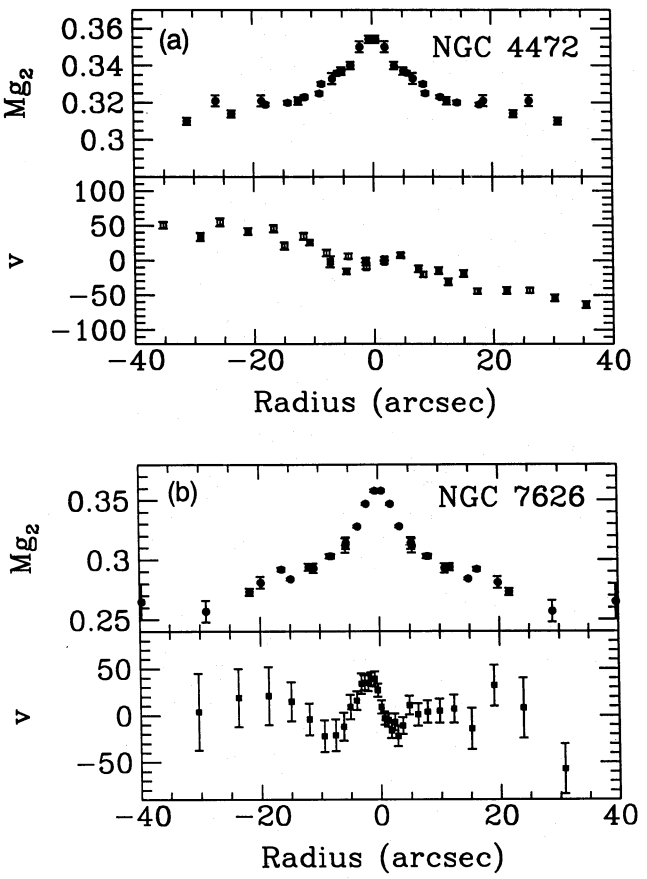

Figure 12. Mg_2 and V_{rot} versus radius for (a) NGC 4472 and (b) NGC 7626. For NGC 7626 we have plotted the major axis (from Jedrzejewski & Schechter 1989) and for NGC 4472 we have plotted $\Gamma = 10°$ (filled symbols from DB) and $\Gamma = 130°$ (open symbols). Note that the values of Mg_2 are reproduced on both sides of the origin.

We find that the contours of constant line strength are the same shape as the isophotes. We find no correlations between the size of the line-strength gradient and any other global parameter of the galaxies such as luminosity or flattening, although our sample is small and spans only a small range in luminosity (about a factor of 10). The correlations between local colours and local line strengths indicate that dust does not play a significant role in the generation of colour gradients in elliptical galaxies.

(2) We confirm the findings of previous workers that the slope of the $\langle Fe \rangle$ versus Mg_2 relation within ellipticals is steeper than the equivalent relation for the nuclei of ellipticals. This can be interpreted as evidence for an enrichment of Mg over Fe compared to the solar values used in the models. Age differences or a younger population cannot be invoked to account for the difference. Mg_2 is created in Type II supernovae with short lifetimes, 10^7 yr, while $\langle Fe \rangle$ arises in Type Ia supernovae with lifetimes of a few $\times 10^9$ years and it is difficult to reduce the amount of iron produced once the bulk of the stars have formed (although if ellipticals have a lower fraction of binary stars there will be fewer Type Ia progenitor stars). Mg_2 could be enhanced with respect to $\langle Fe \rangle$ over the solar value either by enhanced early star formation or by skewing of the initial mass function to produce more massive stars.

(3) We find that Hβ absorption is constant or increases with increasing radius in almost all of the galaxies we observed. Remembering that our sample was chosen to be low-power radio-loud galaxies, and noting that most possess nuclear emission lines, we suggest that the flat or rising profiles arise because the central Hβ absorption is diluted by emission. As the extended emission gets weaker with increasing radius, the Hβ absorption increases. This appears to account for the apparent anomaly of flat or rising Hβ profiles in our sample without the need to invoke the age gradient suggested by FWG for their sample of cluster ellipticals.

(4) We note that, for the five galaxies with ultraviolet colours measured by the *IUE* satellite, there is a tendency for those with the bluest $1550 - V$ colours to have the largest deficiency in Hβ absorption (strongest emission). We speculate that the inverse relationship between Mg_2 and $1550 - V$ reported by Burstein et al. (1988) might be due to the presence of an otherwise undetected blue ionizing nucleus in galaxies with high values of Mg_2. It is perhaps possible that both the activity and the high metallicity result from the star formation associated with the formation of a core.

(5) We have investigated the relationship between metallicity and escape velocity proposed by Franx & Illingworth (1990). Their suggestion, that metallicity is a function of the *local* escape velocity, is confirmed by using Mg_2 as a more direct indicator of metallicity and calculating V_{esc} from the photometry and kinematics of each galaxy. While this result supports the view that abundance gradients and the colour–magnitude relation for ellipticals arise from a common physical cause, the decoupling of Mg_2 and $\langle Fe \rangle$ gradients indicates that other effects, depending on the details of the star formation history, are at work. It seems likely that effects of anisotropy and rotation account for the fact that velocity dispersion is a much poorer indicator of metallicity than is V_{esc}.

(6) NGC 4472 and 7626 have anomalous core kinematics and have line strengths that increase continuously as the radius decreases. The creation of the anomalous cores appears to have been accompanied by star formation that resulted in a stellar population with higher metallicity. The high metallicity of the cores suggests that they are not the remnants of capture of low-mass galaxies, as none of the present examples of possible progenitors reaches the high metallicity levels observed.

ACKNOWLEDGMENTS

We thank Sandra M. Faber, Jesus J. Gonzalez and their collaborators in the Lick Observatory group for making their central values of the line-strength indices available to us at an early stage in this work. We are grateful to Frank Valdes for providing enthusiastic assistance in the use of IRAF to measure line strengths. We gratefully acknowledge the contribution of Marijn Franx who provided tables of V_{esc} for the galaxies plotted in Fig. 11(a). It is a pleasure to acknowledge stimulating discussions on the results of this paper with Ken Freeman, Marijn Franx and Alvio Renzini. We are grateful to the Director of Kitt Peak National Observatory for the allocations of telescope time to complete this work.

REFERENCES

Balcells M., Quinn P. J., 1990, ApJ, 361, 381
Bender R., Surma P., 1992, in Barbuy B., Renzini A., eds, Proc. IAU Symp. 149, The Stellar Populations of Galaxies. Kluwer, Dordrecht, p. 267
Bender R., Burstein D., Faber S. M., 1992, ApJ, 399, 462
Bica E., Alloin D., Schmidt A. A., 1990, A&A, 228, 23
Binney J., Davies R. L., Illingworth G. D., 1990, ApJ, 361, 78
Birkinshaw M., Davies R. L., 1985, ApJ, 291, 32
Boroson T. A., Thompson I. B., 1991, AJ, 101, 111 (BT)
Burstein D., Davies R. L., Dressler A., Faber S. M., Stone R. P. S., Lynden-Bell D., Terlevich R., Wegner G., 1987, ApJS, 64, 601
Burstein D., Faber S. M., Gaskell C. M., Krumm N., 1984, ApJ, 287, 586 (BFGK)
Burstein D., Bertola F., Buson L. M., Faber S. M., Lauer T. R., 1988, ApJ, 328, 440
Caldwell N., 1984, PASP, 96, 287
Carlberg R., 1984, ApJ, 286, 404
Cohen J. G., 1979, ApJ, 228, 405
Couture J., Hardy E., 1988, AJ, 96, 867
Davidge T. J., 1992, AJ, 103, 1512
Davies R. L., Birkinshaw M., 1988, ApJS, 68, 409 (DB)
Davies R. L., Efstathiou G., Fall S. M., Illingworth G., Schechter P. L., 1983, ApJ, 266, 41
Davies R. L., Burstein D., Dressler A., Faber S. M., Lynden-Bell D., Terlevich R., Wegner G., 1987, ApJS, 64, 581
Delisle S., Hardy E., 1992, AJ, 103, 711
de Vaucouleurs G., de Vaucouleurs A., Corwin H., 1976, The Second Reference Catalogue of Bright Galaxies. Univ. Texas Press, Austin
Ebneter K., Balick B., 1985, AJ, 90, 183
Efstathiou G., Gorgas J., 1985, MNRAS, 215, 37P
Elston R., Silva D., 1992, AJ, 104, 1360
Faber S. M., 1977, in Tinsley B. T., Larson R. B., eds, The Evolution of Galaxies and Stellar Populations. Yale University Press, New Haven, p. 157
Faber S. M., Friel E., Burstein D., Gaskell C. M., 1985, ApJS, 57, 711
Faber S. M., Wegner G., Burstein D., Davies R. L., Dressler A., Lynden-Bell D., Terlevich R., 1989, ApJS, 69, 763
Faber S. M., Worthey G., Gonzalez J. J., 1992, in Barbuy B., Renzini A., eds, Proc. IAU Symp. 149, The Stellar Populations of Galaxies. Kluwer, Dordrecht, p. 255 (FWG)
Franx M., Illingworth G. D., 1990, ApJ, 359, L41
Franx M., Illingworth G. D., Heckman T., 1989, AJ, 98, 538
Freedman W. L., 1992, AJ, 104, 1349
Frogel J. A., Whitford A. E., 1987, ApJ, 320, 199
Gilmore G., Wyse R. F. G., Kuijken K., 1989, ARA&A, 27, 555
Gorgas J., Efstathiou G., Aragón Salamanca A., 1990, MNRAS, 245, 217 (GES)
Jedrzejewski R. I., Schechter P. L., 1989, AJ, 98, 147
Jørgensen I., Franx M., Kjaergaard P., 1992, A&AS, 95, 489
Larson R. B., 1976, MNRAS, 176, 31
Matteucci F., 1992, in Capaccioli M., Busarello G., eds, Morphology and Physical Classification of Galaxies. Kluwer, Dordrecht, p. 245
Mould J. R., 1978, ApJ, 220, 434
O'Connell R., 1980, ApJ, 236, 430
Peletier R. F., 1989, PhD thesis, University of Groningen
Peletier R. F., Davies R. L., Illingworth G. D., Davis L., Cawson M., 1990, AJ, 100, 1091 (PDIDC)
Phillips M. M., Jenkins C. R., Dopita M. A., Sadler E. M., Binnette L., 1986, AJ, 90, 1061
Pickles A. J., 1985, ApJ, 296, 340
Rose J. A., 1985, AJ, 90, 1927
Sadler E. M., 1992, in Barbuy B., Renzini A., eds, Proc. IAU Symp. 149, The Stellar Populations of Galaxies. Kluwer, Dordrecht, p. 41
Sandage A. R., Visvanathan N., 1978, ApJ, 223, 707
Statler T. S., 1991, AJ, 102, 882
Tinsley B. M., Gunn J. E., 1976, ApJ, 206, 525
Valdes F., 1986, Proc. SPIE, 627, 749
van der Marel R. P., 1991, MNRAS, 253, 710
van der Marel R. P., Binney J., Davies R. L., 1990, MNRAS, 245, 582
White S. D. M., 1980, MNRAS, 191, 1P
Whitmore B., McElroy D. B., Tonry J., 1985, ApJS, 59, 1
Witt A. N., Thronson H. A., Capuano J. M., 1992, ApJ, 393, 611